Clouds and the Earth's Radiant Energy System (CERES)

Algorithm Theoretical Basis Document

Time Interpolation and Synoptic Flux Computation for Single and Multiple Satellites

(Subsystem 7.0)

David F. Young[1]
Takmeng Wong[2]
Bruce A. Wielicki[2]
Patrick Minnis[2]
Gary G. Gibson[1]
Bruce R. Barkstrom[2]
Thomas P. Charlock[2]
David R. Doelling[1]
Alvin J. Miller[3]
Maria V. Mitchum[2]
Sarah E. Sullivan[4]
Lisa H. Coleman[4]

[1]Analytical Services & Materials, Inc., One Enterprise Parkway, Suite 300, Hampton, Virginia 23666
[2]Atmospheric Sciences Division, NASA Langley Research Center, Hampton, Virginia 23681-0001
[3]Climate Analysis Center, Room 805, NOAA/NWS, Washington, DC 20233
[4]Science Applications International Corporation (SAIC), Hampton, Virginia 23666

June 2, 1997

CERES Top Level Data Flow Diagram

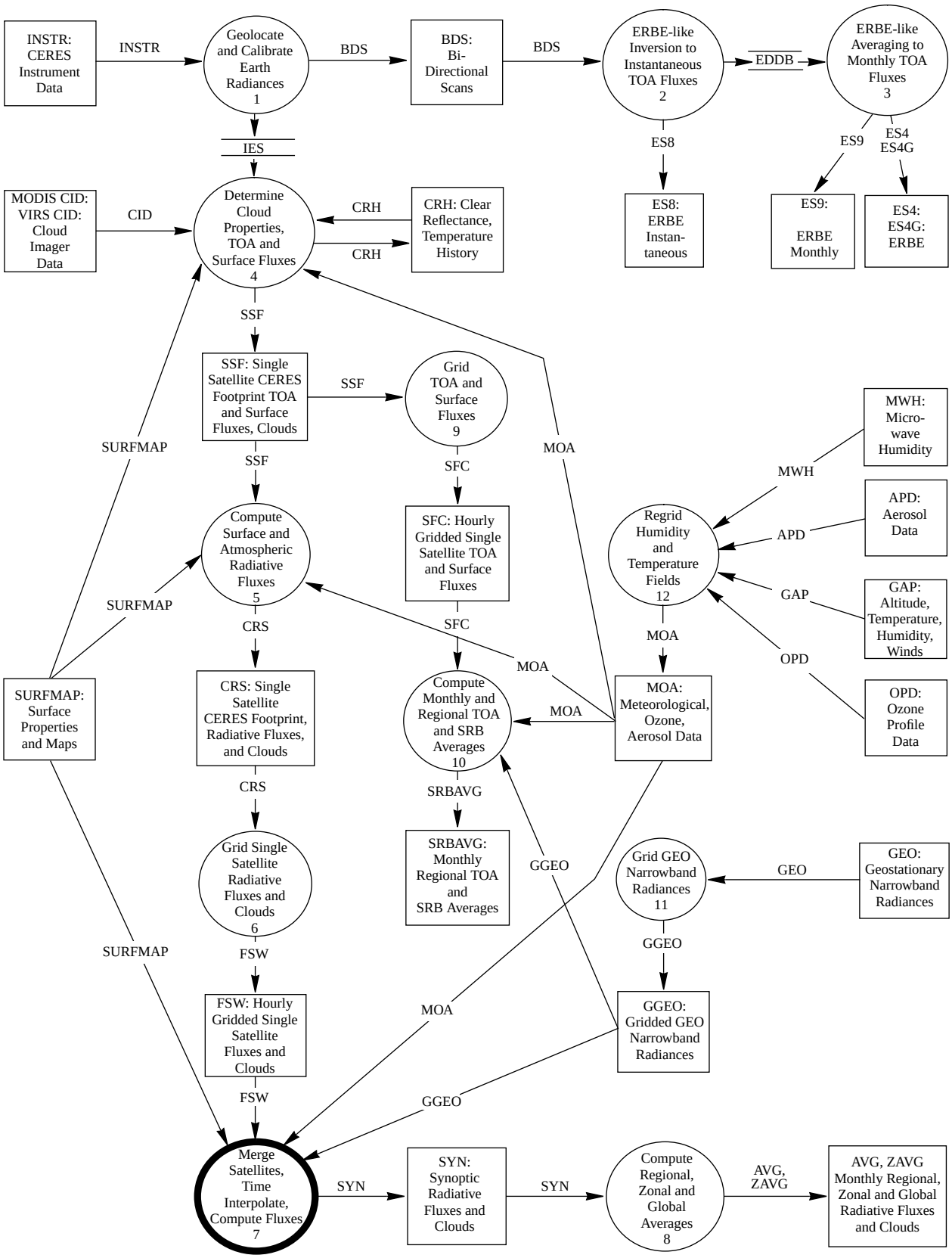

Abstract

The Clouds and the Earth's Radiant Energy System (CERES) Data Management System temporally interpolates CERES data in order to produce global, synoptic maps of top-of-atmosphere (TOA) fluxes and cloud properties on a 1.0° equal-angle grid. These interpolated data are used as input and boundary conditions to the calculation of synoptic maps of the vertical structure of atmospheric and surface flux.

The chief input to the time interpolation process is the gridded shortwave (SW) and longwave (LW) TOA clear-sky and total-sky fluxes and cloud information provided by the FSW data product (see appendix A). These data contain spatial averages of one hour of CERES measurements on a 1.0° equal-angle grid.

This process produces global maps of TOA total-sky LW and SW flux, TOA clear-sky LW and SW flux, TOA window radiances, and cloud properties at 0, 3, 6, ..., 21 GMT for each day of the month. Radiative fluxes at various levels in the atmosphere are then calculated using these data. The final data product contains synoptic maps of the above parameters plus radiative fluxes at four atmospheric levels (see appendix B).

The steps in producing synoptic maps are

1. *Merge gridded cloud and radiation data from multiple satellites*
2. *Regionally and temporally sort and merge ancillary geostationary data used in the interpolation of TOA fluxes*
3. *Interpolate cloud properties from the CERES times of observation to the synoptic times*
4. *Interpolate CERES TOA LW and SW fluxes to synoptic times using geostationary data to assist in modeling meteorological variations between times of observations*
5. *Use time-interpolated cloud properties to calculate radiative flux profiles as in subsystem 5, which are constrained by the synoptic TOA flux estimates*

7.0. Time Interpolation and Synoptic Flux Computation for Single and Multiple Satellites

7.1. Time Interpolation for Producing Synoptic Maps

7.1.1. Introduction

The CERES experiment (Wielicki and Barkstrom 1991) will produce a data set of highly accurate measurements of the incoming and outgoing energy in the Earth's climate system. As with any satellite experiment, the data will not be uniformly distributed in time and space. Instead, data will be arranged in patterns determined by the orbital characteristics of the satellites that are carrying the instruments. However, many researchers prefer data sets that are both global and ordered uniformly in time.

In order to provide such a product for potential data users, CERES will develop global synoptic maps of TOA fluxes and cloud properties as well as the vertical structure of atmospheric radiative fluxes. These maps will be produced for each day of data in 3-hourly intervals at 0, 3, 6, ..., 21 GMT.

Producing data sets for synoptic times ensures consistency with ground truth meteorological observations from weather station observations and radiosondes as well as with geostationary satellites which provide images at synoptic hours. The use of such data is valuable for CERES validation and for science studies using CERES radiation parameters. Also, calculating the atmospheric radiative fluxes at only the synoptic times minimizes the considerable computational resources required for this product. The production of a CERES synoptic data product is important for several reasons: (1) synoptic views provide a basis for studying the life cycle of cloud systems (Desbois et al. 1989; Garand 1988) and understanding the associated atmospheric meteorology, (2) synoptic views are very useful in validating the CERES data processing, particularly of time interpolation, and (3) the synoptic data product provides a regular data structure which simplifies the design of algorithms and operation of the data processing system. In addition to providing a fundamental tool for understanding the organization of cloud systems, synoptic views of cloud and radiation fields provide a major tool for diagnostic work on operational weather forecasting and general circulation models because the analysis fields are produced at synoptic times. Data that have been independently interpreted to such standard times provide stronger tests of the validity of the processes parameterized in the models than do monthly average data. The synoptic fields of radiation and clouds should be particularly valuable in developing and understanding of the role of clouds in the generation and dissipation of available potential energy, since the calculation of this quantity requires integration over approximately horizontal layers within the atmosphere.

For each CERES footprint, information is provided on up to four cloud pressure categories (for a detailed description, see section 4.4.). This cloud information is then used along with ancillary atmospheric sounding data to derive a radiative profile for each footprint consistent with the observed CERES TOA fluxes (subsystem 5). The cloud and radiative parameters are then spatially averaged onto the CERES 1.0° equal-angle grid (subsystem 6). The data must then be temporally interpolated to produce synoptic images. It has been recognized that because of the highly nonlinear quality of the radiative fields, it would be difficult to retain internally consistent radiation fields while interpolating to times without measurements. In order to circumvent this problem, only the TOA total-sky and clear-sky SW and LW fluxes, the window channel radiance, and cloud properties will be interpolated to the synoptic times. The radiative profile will then be recalculated using the TISA-produced fields as constraints (section 7.2.). Monthly means can then be produced by averaging the synoptic fields (subsystem 8).

Time averaging techniques used in previous Earth radiation budget (ERB) satellite experiments such as the Earth Radiation Budget Experiment (ERBE) (Barkstrom 1984; Barkstrom and Smith 1986) concentrated on the combination of measurements and modeling of TOA SW and LW fluxes (Brooks et al. 1986). The CERES time-space averaging algorithm emphasizes and builds upon this strength. The temporal interpolation techniques will produce accurate estimates of TOA flux at the synoptic times; the TOA data are then used as the primary constraint to the radiation field calculations. Estimates of the cloud properties at synoptic times will also be provided for use in radiative transfer calculations. Cloud optical and physical parameters are adjusted during the Surface and Atmospheric Radiation Budget (SARB) calculations to better match the TOA flux constraint.

7.1.2. Algorithm Description

7.1.2.1. Time interpolation philosophy. The ERBE time interpolation method produced the most accurate estimates of monthly mean TOA LW and SW flux currently available (Harrison et al. 1990; Barkstrom et al. 1990). However, numerous simulations by the ERBE Science Team have shown that the ERBE time interpolation technique does not produce daily means and estimates of diurnal variability to the same degree of accuracy. This deficiency could introduce significant errors when producing synoptic maps of TOA flux. The primary difficulties in producing accurate measures on a shorter time scale involve limited temporal sampling and the lack of knowledge of variations in meteorology between measurements.

The problems of limited sampling must be addressed by the time interpolation process. The most severe effects of sparse sampling in the ERBE experiment occurred in the calculation of clear-sky fluxes. Much of this problem arose from the coarseness of the ERBE cloud identification process which systematically underestimated clear-sky occurrence. The improved cloud products for CERES will help alleviate this sampling problem since clear-sky identification will be performed with much greater accuracy. However, during periods when only one CERES instrument is flying, data sparseness can affect even the total-sky flux interpolations.

Of course, the temporal sampling can be improved through the use of multiple CERES instruments aboard different spacecraft. An ideal ERB mission would account for diurnal variability by employing a large fleet of satellites to make measurements at all times of day over all regions. In practice, however, only a limited number of satellites (1–3) are flown and the unsampled hours are filled in with diurnal models or data from other sources. The first CERES mission in 1997 will involve a single satellite (Tropical Rainfall Measuring Mission, TRMM) in 35° inclined orbit providing sampling only twice a day between about 45°N and 45°S. With the 1998 launch of the Earth Observing System (EOS)-AM platform in a Sun-synchronous orbit with an equatorial crossing local time of 1030, the diurnal sampling will increase to 4 times per day. In the year 2000, the EOS-PM platform will be launched into a Sun-synchronous orbit with an equatorial crossing time of 1330. CERES will then have 6 samples per day, assuming EOS-AM and TRMM are operating or their follow-on spacecraft with CERES instruments are launched. Simulation studies using hourly Geostationary Operational Environmental Satellite (GOES) data indicate that the ERBE time-space averaging algorithm gives regional monthly mean temporal sampling errors that are significantly reduced as more satellites are added. For example, the temporal sampling errors in SW flux are reduced from 9 W-m^{-2} for TRMM alone to 4 W-m^{-2} for TRMM plus EOS-AM, and down to 2 W-m^{-2} for TRMM plus EOS-AM and EOS-PM. Since satellites can fail prematurely, it is useful to provide a strategy to reduce time sampling errors, especially for the single satellite case. The CERES strategy is to incorporate 3-hourly geostationary radiance data to account for diurnal cycles which are insufficiently sampled by CERES. The key to this strategy is to use the geostationary data to assist in determining the shape of the diurnal cycle, but use the CERES observations as the absolute reference to anchor the more poorly calibrated geostationary data. One advantage of this method is that it produces 3-hourly synoptic radiation fields for use in testing global models, and for improved examination of the diurnal cycles of clouds and radiation.

CERES can indeed make significant improvements to the ERBE time interpolation process by using ancillary data to provide additional information concerning meteorological changes occurring between CERES measurements. The ERBE Science Team explicitly excluded the use of ancillary data in order to produce a self-contained and relatively straightforward climate data set specifically geared toward accurate measures of monthly mean TOA fluxes. The goals of CERES are more ambitious than ERBE. In addition to the products delivered by the ERBE experiment, CERES also provides extensive analyses of cloud properties as well as surface and atmospheric radiation parameters. In order to calculate these parameters, it is necessary to use ancillary data such as moderate resolution imaging spectroradiometer (MODIS) or Visible Infrared Scanner (VIRS) radiance data, atmospheric structure data, and constantly updated background surface data (see subsystem 4).

In order to meet the CERES goal of improved temporal averaging, numerous simulations were performed to explore techniques of incorporating additional data sources into the time averaging process. Since the main requirement of such data is to have enhanced temporal resolution, an obvious candidate data source is geostationary and polar-orbiting satellite radiance measurements. Geostationary data from such satellites as GOES, METEOSAT, INSAT, and GMS provide measurements of narrowband visible and infrared radiances for much of the globe (~50°N to 50°S) at a temporal resolution as fine as every hour. The polar-orbiting satellites provide much less temporal information, but are useful for providing information at higher latitudes.

Because of the excellent temporal resolution of geostationary data, many attempts have been made to derive broadband radiation budget parameters from these narrowband measurements (Minnis et al. 1991; Briegleb and Ramanathan 1982; Doelling et al. 1990). Generally, these studies have demonstrated that the narrowband measurements are insufficient for radiation budget calculations since they miss valuable spectral information contained in broadband observations. Minnis et al. (1991) showed that the LW narrowband-broadband relation varied significantly in time and space even when water vapor, surface type, and cloud data were considered. Figure 7.1-1 shows regional means and standard deviations of the differences between ERBE measured LW fluxes and broadband fluxes derived from GOES narrowband measurements using a global correlation that includes an atmospheric water vapor term. The overall relative error of the correlation is ~11 W-m^{-2} and mean biases greater than 15 W-m^{-2} are evident in many regions. Regressions performed on a region-by-region basis can reduce the relative error to 7.7 W-m^{-2}, and essentially eliminate the mean bias. However, these regional correlations require frequent updating to account for changes in calibration and seasonal variations in the narrowband-broadband relation. Thus, narrowband data should be used in climate studies only if the narrowband-broadband relationship is continually calibrated using coincident measurements with a broadband instrument such as CERES.

While narrowband measurements cannot be used directly for radiative studies, these data contain valuable information that can be used with a broadband monitoring satellite system such as CERES. In particular, these measurements provide a glimpse at the variations in meteorology occurring between the times of CERES observations. Several simulations have demonstrated that judicious use of geostationary data can enhance the accuracy of time interpolation of broadband observations. The techniques that produce the most accurate averages are described below.

For release 2.1, cloud conditions are assumed to vary linearly with time when producing input to the synoptic radiative transfer calculations. Since only radiances and no cloud information are provided by the narrowband data at synoptic times, all cloud information will necessarily be derived solely from the CERES analysis of MODIS or VIRS observations. Since this approach will, at times, produce cloud conditions that are inconsistent with the interpolated TOA fluxes, these cloud properties will be adjusted during the atmospheric flux calculations to obtain agreement between the interpolated and calculated TOA fluxes. In this way, monthly means can be computed from the synoptic grids of radiatively balanced data.

7.1.2.2. Organizing and merging spatially gridded observations. The first step in the time interpolation process is to accumulate and organize the observed CERES data. The primary input to the computation of synoptic maps is the gridded CERES SW and LW TOA fluxes and cloud information provided by the FSW data product. This input consists of regionally and temporally sorted averages of CERES measurements for each observed region of the 1.0° equal-angle grid (see appendix A). As with the ERBE-like monthly time-space averaging product (see subsystem 3), one month of data will be processed together. In addition, each region will be analyzed independently of all others.

At this point in the processing, data from instruments on different satellites are combined. Whenever multiple-satellite data are available, measurements from all sampled hour boxes are used in the averaging process and the number of input files increases proportionally. When data exist for a given hour and region from more than one satellite, the data are linearly averaged.

The process of sorting and merging these data is very similar to that used in the processing of the ERBE-like data. The major difference is that the CERES grid contains approximately six times as many regions as used by ERBE. Fortunately, only a small number of the parameters from the FSW files need to be retained in this step. The relevant parameters from FSW which are used in the averaging process are the total-sky LW and SW TOA fluxes, the clear-sky TOA LW and SW fluxes, and the CERES-derived cloud information.

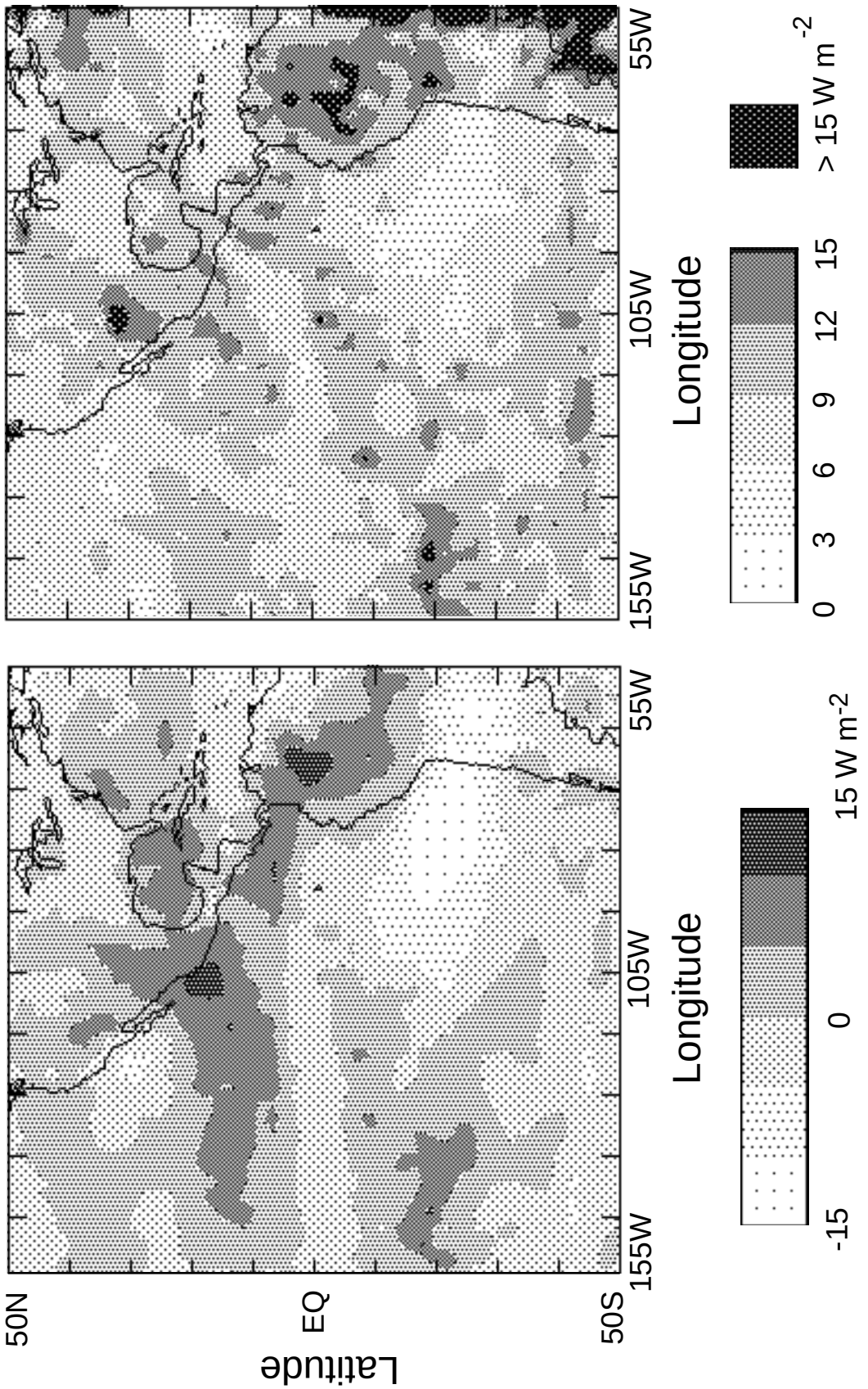

(a) Means.

(b) Standard deviations.

Figure 7.1-1. Regional means and standard deviations of the differences between ERBE broadband LW fluxes and inferred broadband fluxes derived from GOES narrowband IR radiances.

7.1.2.3. Regridding of geostationary data. Since geostationary data will be used in both Subsystems 7 and 10, the regridding of these data on to the CERES 1.0° equal-angle grid has been designated as a separate subsystem (11.0). For details, see the ATBD for this subsystem.

7.1.2.4. Time interpolation of cloud properties. CERES will advance the understanding of the Earth's radiation budget through a more detailed description of the effects of clouds. Extensive information concerning the physical and radiative properties of clouds is provided with each CERES footprint. After the CERES footprints are sorted and averaged onto the CERES 1.0° equal-angle grid, these cloud data will be binned and stored in four separate data structures. These data structures, which are discussed in detail in section 4.4. and subsystem 6, are reviewed here for clarity since each is necessary as input for different aspects of time interpolation.

The cloud imager data have been sorted primarily as a function of cloud-top pressure. Four main pressure categories have been identified for use throughout the CERES Data Management System: low (P > 700 hPa), lower middle (700 hPa > P > 500 hPa), upper middle (500 hPa > P > 300 hPa), and high (P < 300 hPa). The vertical spacing of these categories (~3 km) allows the assumption that the cloud properties of these four categories can be spatially and temporally averaged independently. From these four categories, 11 cloud conditions are possible: clear, the four categories occurring as single layer clouds, and the six possible two-layer conditions (high over low, etc.).

The first cloud data structure, denoted as cloud overlap conditions, is simply a vector of frequency of occurrence for each of the 11 possible cloud conditions.

The second data structure is cloud category properties, which contains the means and standard deviations of each of the cloud properties detailed in table 4.4-3 for each of the four cloud pressure categories.

The third data structure is column-averaged cloud properties. These data are averaged using five different weighting schemes that reflect the needs of different potential users of CERES data. Separate statistics using different averaging schemes are to be compiled for two main groups of users. The first group of users is the atmospheric radiation community. These researchers are interested in studying the effects of changes in cloud radiative forcing. In order to conserve radiative properties during the averaging process, parameters saved for this group should be weighted by their effect on cloud radiative forcing. The second group of CERES users is the atmospheric dynamics community. These researchers are interested in cloud generation/dissipation parameterizations to be used in general circulation models. In contrast with the averaging used to preserve radiative features, average properties to be used by this group of researchers should be weighted by the liquid or ice water volume in a region. The details of the five weighting schemes are described in subsystem 6.

The fourth cloud data structure is the angular model scene class. This structure is analogous to the scene fraction and albedo arrays provided for each hour box in the ERBE-like processing. Scene fraction, mean albedo, mean LW flux, and mean incident solar flux are provided for each angular distribution model (ADM) class. For release 2.1, the ADM classes are limited to the twelve ERBE scene types (Suttles et al. 1988 and 1989). For later releases, new ADM's will be developed as discussed in section 4.5.

The interpolation of these cloud data to synoptic times is performed using three main assumptions:

1. The properties of the four cloud pressure categories can be interpolated independently
2. Cloud properties for each region will be interpolated independently from surrounding regions
3. Variations in cloud properties between CERES observation times will be modeled as linear

The linear variation assumption is applied in one of two ways, depending on the cloud conditions of the two points between which the interpolation is performed. If a nonzero cloud amount exists for a given cloud pressure category at both times, then the means and standard deviations of all cloud proper-

ties are linearly interpolated with respect to time. This case is illustrated in figure 7.1-2a. The sole exception to this is the visible optical depth, which is recalculated from the interpolated values of liquid (or ice) water path and particle size using the relationships described in subsystem 4. If, however, only one of the two observation times contains a nonzero cloud amount for the cloud category, then only cloud amount is linearly interpolated. As shown in figure 7.1-2b, the remaining properties are assumed to be constant throughout the time period, but the cloud simply reduces in area coverage as if it were advecting out of the region.

The averaging techniques are performed on each of the four cloud data structures. The first two structures, the cloud overlap conditions and the cloud category properties, are used as initial conditions of the radiative transfer calculations. The fourth structure is used in the TOA SW flux interpolation process to provide information for the selection of ADM's used with broadband fluxes derived from geostationary narrowband SW data. The column-averaged data are not used in the production of the synoptic radiative fields, but are recalculated from the synoptic data and later averaged in subsystem 8.0 to produce monthly mean information concerning the cloud conditions associated with the radiation budget.

7.1.2.5. Time interpolation of total-sky TOA LW flux. The TOA LW flux is interpolated to the synoptic times in one of two ways. The first, termed method 1, is identical to the technique used in the ERBE-like processing. This technique, which uses a combination of linear interpolation and idealized diurnal models, is described in subsystem 3. An example of results using this method are given in Harrison et al. (1988).

The chief improvement proposed for method 2 is the inclusion of narrowband geostationary satellite-derived information. Instead of the combination of linear interpolation and idealized half-sine curves used by the ERBE-like technique to fit the observations, method 2 uses narrowband data to provide a more accurate picture of the shape of the curve that is fit to the observations.

For release 2.1, method 2 is used whenever possible. However, geostationary data are not available for all latitudes, and occasional gaps can occur in the data record (such as the unavailability of INSAT data). Whenever narrowband data are not available or are inadequate, the TOA fluxes are derived using method 1.

Narrowband radiances are transformed into broadband fluxes using the regression techniques developed by Minnis et al. (1991). The regression is derived from coincident calibrated geostationary and CERES measurements and ancillary relative humidity data available from the ASTR atmospheric data set. The form of the regression is:

$$F_{bb} = a_0 + a_1 F_{nb} + a_2 F_{nb}^2 + a_3 F_{nb} \ln(rh) \tag{7.1-1}$$

where F_{bb} is the LW broadband flux, F_{nb} is the narrowband flux, rh is the column-averaged relative humidity, and a_i are the derived coefficients. The LW narrowband radiance is converted to narrowband flux by:

$$F_{nb} = \frac{6.18 I_{nb}}{\gamma(\theta)} \tag{7.1-2}$$

where I_{nb} is the LW narrowband radiance, $\gamma(\theta)$ is the longwave limb-darkening function at viewing zenith angle θ, and 6.18 represents the product of the limb darkening function integrated over an entire hemisphere and the narrowband spectral interval (Minnis et al. 1991).

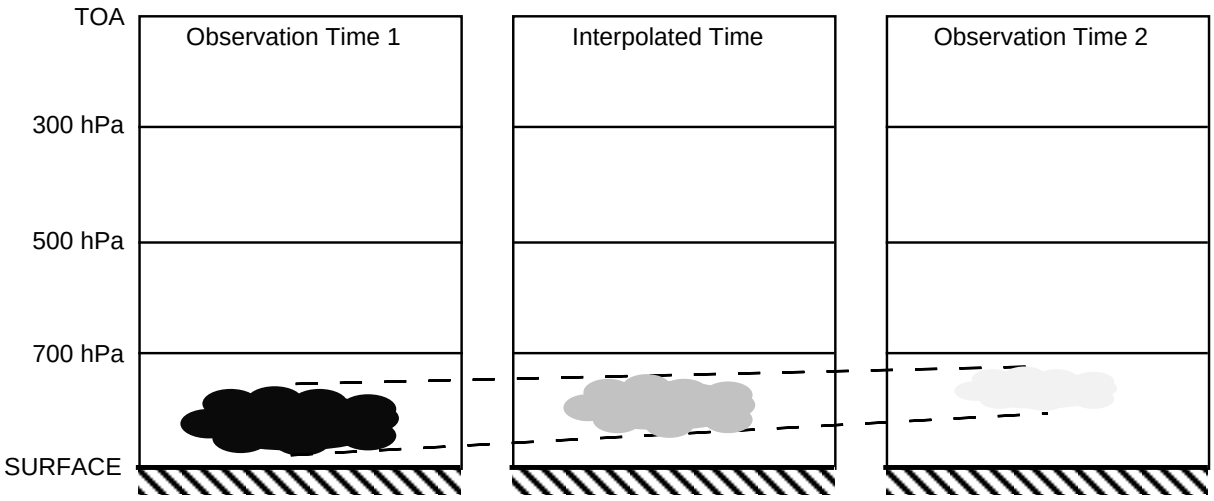

(a) Cloud properties are linearly interpolated between two cloud observation times.

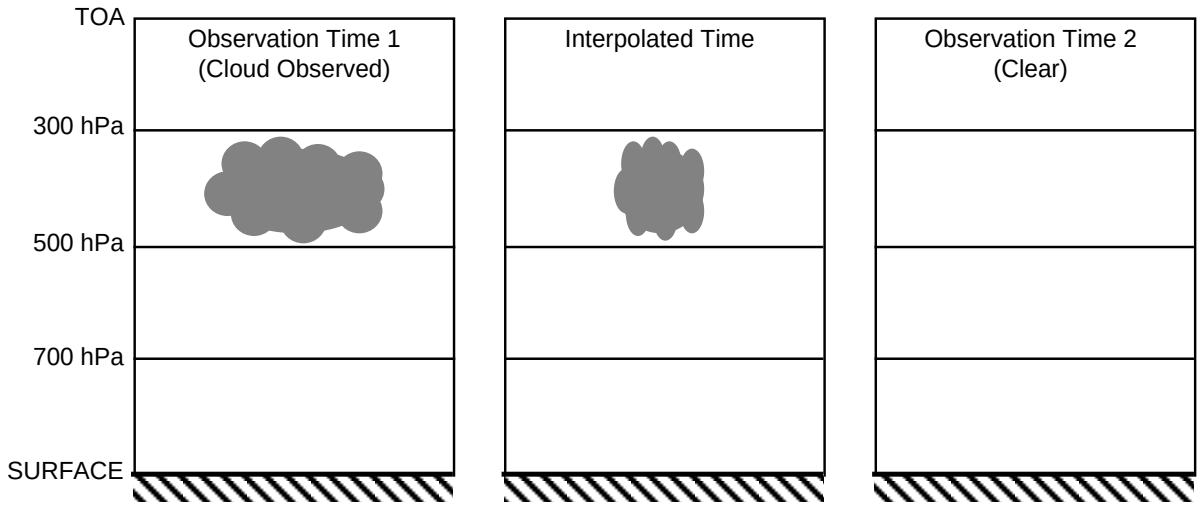

(b) All properties except cloud amount are assumed constant between cloud observation time 1 and clear observation time 2.

Figure 7.1-2. Temporal interpolation of cloud properties.

As discussed above, Minnis et al. demonstrated that there is significant variability in the narrowband-broadband relationship both regionally and temporally. In order to account for temporal variability, the regressions are rederived each month using global data. Separate correlations are performed for ocean and land regions. Since the derivation of separate regressions for each CERES region for each month of data may not be feasible, another technique is required to account for regional variations in the correlation. Once a complete time series of simulated broadband measurements is constructed for the region, the derived LW fluxes at all hours are normalized to the nearest CERES observation of flux. This renormalization is sufficient to reduce the residual regional variance from the narrowband-broadband regression. For points between two CERES measurements, the normalization is linearly scaled inversely by the time difference between the hour in question and the times of the observations.

The renormalization of the broadband LW curve derived from the narrowband radiances to the nearest CERES observation assures that the final diurnal variability assumed in the time interpolation process is directly tied to the measured fluxes. This process also will reduce any errors incurred by variations in the calibration of the narrowband instruments. The narrowband data are used simply to provide extra information concerning meteorological variations between the measurements. As more than one CERES instrument becomes operational, the reliance on the narrowband data to provide the diurnal shape will diminish. With the improved time sampling, the interpolated curves will be dominated by the CERES observed fluxes.

Several studies have been performed to demonstrate the benefits of incorporating narrowband measurements into the averaging process (Harrison et al. 1994). Past studies have shown that the use of techniques such as the half-sine fit used by ERBE over land regions is more effective than linear interpolation in reproducing the LW diurnal variability seen in narrowband measurements (Brooks and Minnis 1984). Studies such as these rely on using 1-hourly GOES data converted to broadband flux using narrowband-broadband regressions as a reference data set. The effects of sampling patterns and the relative errors inherent to various interpolation schemes can be evaluated by sampling this reference set and comparing the results of the interpolation with the reference set.

Unfortunately, in order to show an improvement in interpolation using method 2, it is necessary to have three independent data sets: the broadband measurements, the narrowband time series, and an additional broadband reference data set. Since the GOES data are used in the averaging process, it is improper to use GOES as the reference data set. In addition, there is no 1-hourly global broadband data set to use as the truth.

This problem is overcome by using ERBE data from two different satellites, ERBS and NOAA-9, as two independent data sets. Observations from one satellite are interpolated to the observation times of the other using four different techniques (denoted as techniques a–d). Technique (a) is the ERBE-like combination of linear and half-sine interpolation of method 1. The geostationary-data-enhanced technique described above is performed in three ways. The first, (b), uses 1-hourly GOES data as a best-case test. The second approach, (c), uses the 3-hourly time sampling that is most likely to be available during CERES processing. Finally, in method (d), ERBE measurements are predicted simply using the 3-hourly narrowband measurements converted to broadband using the regression fit, but without the normalization to ERBE to account for regional variations. This method is included to demonstrate the necessity of continually anchoring the narrowband-derived fluxes to the measurements in order to produce the most accurate time-averaged fluxes possible.

A comparison of two of these techniques, (a) and (c), is displayed in figure 7.1-3 for an ERBE 2.5° region over New Mexico during the first 15 days of July 1985. The top curve shows the ERBE-like technique (a), and the bottom curve is the normalized 3-hourly narrowband shapes technique (c). In both figures, ERBS observations of TOA LW flux are displayed as solid squares and NOAA-9 observations are open circles. The interpolation techniques were applied to the NOAA-9 data in order to predict the ERBS observations. Both techniques do a good job on days with adequate sampling and constant cloudiness such as days 6–8 and 10–12. However, the ERBE TSA severely misses several nighttime points during the first three days of the period, as well as daytime points on days 6 and 14. Method (c), however, does a much improved job of filling in the fluxes in the hours between the observations. In particular, the predicted daytime fluxes on day 5 and the nighttime fluxes on days 1–4 are closer to the ERBS values. A few ERBS fluxes have been missed because of the 3-hour time resolution of the narrowband data, but, overall, method (c) shows a substantial improvement over method (a).

The results for the four interpolation techniques are summarized in table 7.1-1 for all 2.5° regions between 50°N–45°S latitude and 155°W–55°W longitude during the entire month of July 1985 and between 50°N–45°S latitude and 145°W–45°W longitude during April 1985. The first row of the table contains a comparison of coincident ERBS and NOAA-9 ERBE observations. Data from all regions

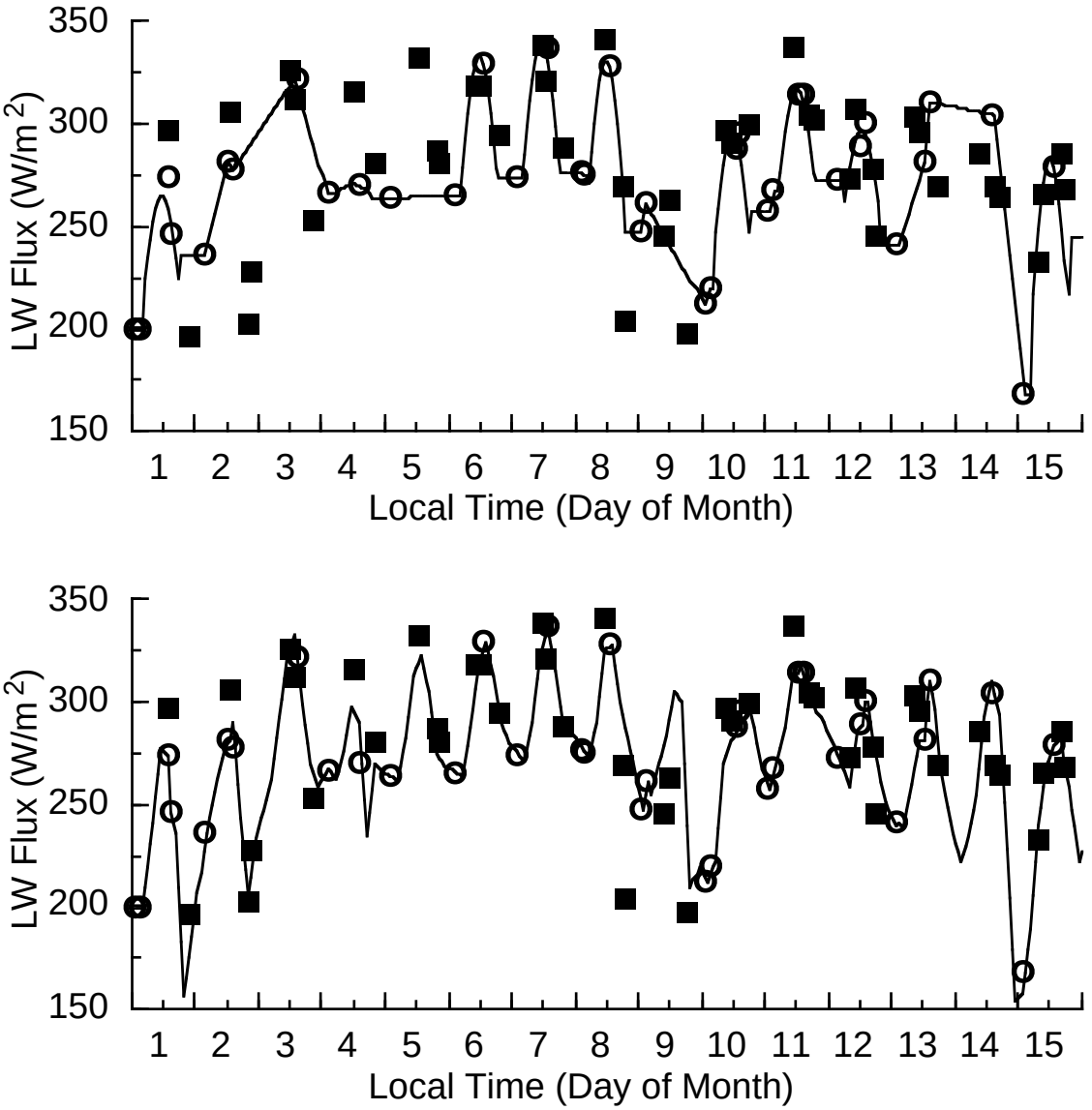

Figure 7.1-3. Time series of ERBE ERBS (■) and NOAA-9 (❍) LW flux observations and interpolated values from July 1985 over New Mexico. The top curve shows the ERBE time interpolated values; the bottom curve shows the geostationary-data-enhanced interpolation.

viewed by both ERBE instruments during the same hour are included. Since this comparison is performed using data averaged in coincident hour boxes, any difference between the two can be due to a combination of temporal and spatial variations within the 2.5° region over one hour as well as miscalibration between the two instruments or errors in the ADM's used to convert the radiances to fluxes. A 2.4 W-m^{-2} bias and 10.6 W-m^{-2} instantaneous rms error (difference) exists between the two data sets in July. The April data show similar values of –0.1 ±10.0 W-m^{-2}. An estimate can be made of the magnitude of the errors due to the ADM's. When the two instruments view the scene with viewing zenith angles within 10° of each other, the rms differences are reduced to 5–6 W-m^{-2} for both months while the biases remain unchanged.

Although the overall biases are small (less than 1% of the mean flux), they are significant to this study. The results of the various time interpolation schemes must be compared with these coincident biases. A perfect time interpolation should not produce a zero bias, but rather should reproduce the bias in the coincident ERBS and NOAA-9 data.

Table 7.1-1. Comparison of LW Flux Time Interpolation Techniques Using ERBE Data From (a) July 1985 and (b) April 1985. Instantaneous Mean and rms Differences (W-m^{-2}) Between NOAA-9 LW Flux Measurements and Fluxes Predicted From ERBS Observations

(a) July 1985	NOAA-9 mean flux	Total error		Time interpolation error	
		Mean	rms	Mean	rms
Coincident data	243.6	2.4	10.6	-	-
a) ERBE TSA	246.5	2.8	16.9	0.4	13.2
b) w/ 1-hourly GOES	246.5	3.1	11.4	0.7	4.2
c) w/ 3-hourly GOES	246.5	2.8	12.0	0.4	5.6
d) Non normalized/3 hr	246.5	2.6	14.4	0.2	9.7

(b) April 1985	NOAA-9 mean flux	Total error		Time interpolation error	
		Mean	rms	Mean	rms
Coincident data	246.6	–0.1	10.0	-	-
a) ERBE TSA	246.2	0.7	15.7	0.8	12.1
b) w/ 1-hourly GOES	246.2	0.8	11.3	0.8	5.3
c) w/ 3-hourly GOES	246.2	0.7	11.8	0.7	6.3
d) Non normalized/3 hr	246.2	0.2	14.9	0.2	11.0

The successive rows of table 7.1-1 show the capability of each interpolation technique to reproduce the NOAA-9 observations by temporally interpolating the ERBS data. The mean LW flux from NOAA-9 is provided in column 1. The next two columns contain the absolute instantaneous mean and rms difference between the observed NOAA-9 flux and the flux predicted for that hour by interpolating the ERBS observations. Estimates of the mean and rms error from the time interpolation processes have also been included in columns 4 and 5. The rms due to time interpolation is calculated assuming that the time interpolation error is independent of the rms difference between coincident ERBS and NOAA-9 measurements. It is calculated as:

$$rms_{ti}^2 = rms_T^2 - rms_o^2 \tag{7.1-3}$$

where rms_T is the total rms from the technique, rms_{ti} is the rms of the time interpolation technique, and rms_o is the rms from comparison of coincident ERBS and NOAA-9 observations. The mean time interpolation error is simply the difference of the total mean error and the mean difference in the coincident fluxes.

It is apparent that the lowest rms errors are obtained using narrowband data with 1-hour temporal resolution. However, there is only a slight (1–2 W-m^{-2}) degradation in the rms error when 3-hourly data are used. There is, however, a substantial improvement in the time interpolation error using the GOES data over the ERBE time averaging scheme. The rms error due to time interpolation decreases from 13.2 W-m^{-2} to only 5.6 W-m^{-2} for the July data and from 12.1 W-m^{-2} to 6.3 W-m^{-2} for April. In addition, the mean bias is less than 1 W-m^{-2} for all cases.

Clearly, the renormalization process is necessary for accurate temporal interpolation. Method (d) simply used the narrowband-broadband correlations to produce the LW flux time series from the GOES data. The instantaneous time interpolation rms error is increased from 5.6 W-m^{-2} to 9.7 W-m^{-2} in July and from 6.3 W-m^{-2} to 11.0 W-m^{-2} in April. The latter error is only a minimal improvement over the ERBE-like method (a). Through renormalization, the time series of LW flux is accurately tied to the original observations. Region-to-region variations in the narrowband-broadband correlations and temporal variations in the narrowband calibration are properly accounted for.

The statistics presented above from these simulations have related to the errors involved in the prediction of instantaneous fluxes. The changes in the temporal interpolation process being proposed here are mainly for improving these instantaneous estimates of flux. It is crucial that any proposed time interpolation technique does not significantly affect the monthly means. Harrison et al. (1990) demonstrated that ERBE regional monthly mean LW flux estimates are accurate within 1 W-m^{-2} if data from two satellites are used. For July, over the entire GOES region, the ERBE method (a) produces monthly mean flux averaged over all regions of 249.0 W-m^{-2}. For methods (c) and (d), the averages are 248.8 W-m^{-2} and 248.4 W-m^{-2}, respectively. Thus, the enhancements to the interpolation process are not adversely affecting the monthly means. Once again, the anchoring of the LW fluxes to the observations in method (c) produces an improvement over the results of method (d).

Another advantage in the use of narrowband data for the interpolation process is that sampling effects are minimized. This is demonstrated by examining the difference in regional monthly mean fluxes calculated using the two ERBE instruments. The polar-orbiting NOAA-9 satellite produces ERBE sampling near 0230 and 1430 local time throughout the month. The local time of observations from the precessing ERBS satellite slowly changes during the month. The region-to-region rms difference between the monthly mean estimates from the two satellites is a measure of independence of the interpolation to sampling effects. For April, when the mean difference between the two data sets is nearly zero, the regional rms difference in monthly mean is 2.4 W-m^{-2} for method (a) and 1.7 W-m^{-2} for method (c). As expected, the incorporation of the time series of narrowband data increased the accuracy of filling in flux values for times between measurements.

Since the lowest interpolation errors are associated with the method that involves 1-hourly narrowband data, any changes to the other techniques that better simulate the 1-hourly narrowband time series from the 3-hourly data should also improve broadband interpolation. Therefore, additional simulations can be performed solely in the narrowband to see which technique best recreates the 1-hourly data set. For these future studies, the complete GOES data set will be used as a reference. Interpolation errors from these studies can only be interpreted as relative errors; the total error is a combination of the errors in simulating the 1-hourly set from the 3-hourly plus the errors in interpolating broadband fluxes from the 1-hourly data.

Future simulations will also use data from December 1986, which is the only month to have three ERBE scanning instruments operating simultaneously. These data can be used to study the advantages of a two-satellite system by using data from the two sun-synchronous ERBE satellites to predict the ERBS observations.

7.1.2.6. Time interpolation of clear-sky TOA LW flux. The ERBE-like averaging technique does not yield clear-sky flux estimates for all hours of the month. The relative scarcity of clear-sky flux estimates derived from ERBE data necessitated the use of monthly-hourly fits instead of continuous interpolation. Since much of the CERES effort is geared toward studying the effects of clouds on the Earth's radiation budget, there will be a significant improvement in the quality of clear-sky data. The misclassification of clear scenes as partly cloudy will no longer be a problem.

Because of these improvements to the CERES clear-sky data set, time interpolation of clear-sky LW flux is performed in a manner identical to the total-sky product. The lack of geostationary data is not serious in the case of clear-sky modeling. The main information provided by the narrowband data is changes in meteorology and cloudiness. For clear-skies, the idealized ERBE models work well and will be used in release 2.1.

One consideration for the input to the radiative transfer calculations to be performed on the synoptic maps is that clear-sky TOA LW flux is necessary at each synoptic time. Unfortunately, there may be no clear-sky measurements within a day of the desired time. In these cases, clear-sky fits from the nearest day with data will be used.

7.1.2.7. Time interpolation of total-sky TOA SW flux. The decision not to use auxiliary data to assist in the time interpolation of ERBE data not only affected the LW flux means, but also caused similar deficiencies in the SW interpolation process. Between the times of ERBE observations, an assumption of constant or linearly varying cloud conditions was made for all interpolations. This, of course, can lead to biases in the data, particularly in the case of a single satellite-borne instrument measuring SW flux only once each day. Monthly-hourly SW flux estimates for areas with persistent diurnal variations of clouds such as tropical cumulus or coastal stratocumulus regions can have significant errors (Minnis and Harrison 1984). As is the case with LW flux, method 1 for interpolating SW flux is analogous to the ERBE-like interpolation process and method 2 incorporates narrowband geostationary data to provide information concerning changing meteorological conditions between CERES measurements.

The averaging of SW data is not as straightforward as LW data. Unlike the LW flux case, the SW flux interpolation process is heavily dependent upon models. First, anisotropic effects must be accounted for using bidirectional reflectance models. Secondly, whenever averaging data spatially or temporally, all of the data must be adjusted to a common solar zenith using ADM's. For release 2.1, the ERBE ADM's will be used. The ADM's provide a description of the variation of broadband albedo with changing solar zenith angle. As long as cloud conditions remain constant, SW flux can be temporally interpolated accurately. For regions with diurnal variations in cloudiness, information concerning the variation in cloud conditions must also be available to temporally interpolate TOA SW flux properly.

As stated above, method 1 for SW flux is based upon the ERBE-like SW flux interpolation process described in subsystem 3. Separate means of albedo are stored in the angular model scene class cloud data structure along with scene fraction for each ADM class. Each ADM class albedo is interpolated to the synoptic time using the related ADM. The scene fractions are linearly interpolated to the synoptic time and then used to combine the individual albedos into a single total scene albedo. The SW flux is then computed by multiplying the total albedo by the incident solar flux for that time. The chief difference with the ERBE-like process is that a varying surface type is allowed within a CERES region, whereas ERBE assumes that the surface scene is constant for the month. Thus only four possible ADM classes are used in ERBE, but a single CERES region could possibly include all twelve. This change should not increase time interpolation error and, in fact, should produce a more accurate selection of ADM's.

The introduction of narrowband data into the SW flux interpolation process is more complicated than for the LW. In addition to the problem of simulating broadband fluxes from narrowband measurements as is done with the LW, the narrowband SW radiances must also be converted into fluxes using the proper ADM's. However, the improvement in temporal interpolation derived from the increased information concerning meteorology changes outweighs the narrowband-broadband flux calculation errors. Variations in cloudiness have a much greater impact on the SW. A change from a 100% clear scene to 100% overcast may result in a decrease in LW flux of 20–30%, but total-scene albedo may increase by 400–500%. Thus, the increased knowledge gained from the geostationary data concerning changes in clouds can be crucial to improving time interpolation.

The first step in SW method 2 is the time interpolation of the CERES cloud properties as described in section 7.1.2.4. Once the angular model scene class cloud data are interpolated to each synoptic time, the narrowband radiances are converted to narrowband albedos using the CERES ADM's.

$$\alpha_{nb} = \frac{(\pi I_{nb} / S_v \cos\theta_o)}{\left(\sum_{i=1}^{12} R_i \alpha_i f_i / \sum_{i=1}^{12} \alpha_i f_i i \right)} \tag{7.1-4}$$

where α_{nb} is the narrowband albedo, I_{nb} is the mean narrowband SW radiance within the CERES region, S_v is the Earth-Sun distance-corrected narrowband solar constant (which has a nominal value of 526.9 W-m^{-2}sr$^{-1}\mu$m^{-1} , and α_i, f_i, and R_i are the CERES albedo, scene fraction, and bidirectional anisotropic factor for ADM class *i*, interpolated to the synoptic time. Note that these albedos, α_i, are only initial estimates used solely for more accurately weighting the mean anisotropic factor necessary for the calculation of the total albedo. The CERES broadband anisotropic factors are used in this calculation. Doelling et al. (1990) showed that the use of ERBE broadband anisotropic factors in the calculation of albedos from GOES measurements did not degrade the regressions between GOES and ERBE albedos.

The narrowband albedos are converted to estimates of broadband albedos using regressions of the form used by Doelling et al. (1990):

$$\alpha_{bb} = b_0 + b_1\alpha_{nb} + b_2\alpha_{nb}^2 + b_3\ln(\sec(\theta_0)) \qquad (7.1\text{-}5)$$

where α_{nb} is the narrowband albedo, α_{bb} is the broadband albedo, and θ_o is the solar zenith angle at the center of the region at the synoptic time. Separate regressions are performed for ocean and land regions.

A time series of broadband albedos calculated from narrowband measurements in the above manner can still contain significant errors (see Doelling et al. 1990; Briegleb and Ramanathan 1982). Doelling et al. found that regressions of the form of 7.1-5 have rms regression errors in excess of 14%. In addition, strong region-to-region variations in the relationship exist. The truest measurements of broadband SW flux are derived from broadband instruments such as CERES. A time series constructed from narrowband measurements can only be used as a guide for accounting for changes in cloud conditions between the CERES observation times. As with the use of narrowband data in the LW flux interpolation process, it is imperative that the narrowband data not dominate the averaging process. Therefore, the time series must be normalized to the CERES broadband observations.

The accuracy of this interpolation technique was tested in a fashion similar to the LW technique. ERBE measurements from ERBS were used to predict SW flux values measured from NOAA-9 using three techniques. The first (a) is the ERBE technique. The other techniques employ narrowband SW radiances from GOES. The difference between the techniques is in the cloud data used to select the ADM's necessary to convert the narrowband radiances into fluxes. The interpolation is first done using cloud amount, and cloud and clear reflectances derived from the narrowband data using the hybrid bispectral threshold method (Minnis et al. 1987). The results from this technique represent best case examples and are labeled (b) and (c) when applied to 1-hourly and 3-hourly GOES data, respectively. The next two techniques, (d) and (e), use linearly interpolated ERBE cloud amounts and albedos to select the proper anisotropic factor. Technique (d) uses 1-hourly GOES data; technique (e) uses 3-hourly data. These methods are closer to the technique that will be used in release 2.1. A final method (f) is identical to method (e), but does not include the re-normalization of the narrowband-derived fluxes to the nearest observation.

The results are shown in table 7.1-2. As is the case with the LW flux, there is a significant bias between coincident ERBS and NOAA-9 measurements. For July, the instantaneous mean difference is 5.2 W-m^{-2}, with a 36.5 W-m^{-2} rms. For April, the values are 5.1 ±39.1 W-m^{-2}. These differences are much larger than the corresponding values associated with the LW flux. This is due to the greater dependence on ADM's for deriving SW flux from the observations. When the coincident comparison is limited to times when both instruments are viewing within 20° of nadir, the mean bias in July is –1.4 W-m^{-2} and the rms difference falls to only 13.1 W-m^{-2}, which is of the same magnitude as the longwave. Unfortunately, the additional errors associated with model selection hamper some of the comparisons in the simulations. Since the mean differences of even coincident data are strongly angle dependent, it is difficult to determine the absolute accuracy of the averaging techniques. However, the

Table 7.1-2. Comparison of SW Flux Time Interpolation Techniques Using ERBE Data From (a) July 1985 and (b) April 1985. Instantaneous Mean and rms Differences (W-m^{-2}) Between NOAA-9 LW Flux Measurements and Fluxes Predicted From ERBS Observations

(a) July 1985	NOAA-9 mean flux	Total error		Time interpolation error	
		Mean	rms	Mean	rms
Coincident data	259.4	5.2	36.2	-	-
Scaled coincident data	228.5	4.6	32.2	-	-
a) ERBE TSA	228.5	0.0	53.8	–4.6	43.1
b) w/ 1-hourly GOES + GOES clouds	228.5	–1.0	35.1	–5.6	14.1
c) w/ 3-hourly GOES + GOES clouds	228.5	–0.8	36.0	–5.4	16.2
d) w/ 1-hourly GOES + ERBE clouds	228.5	6.2	39.5	1.6	22.9
e) w/ 3-hourly GOES + ERBE clouds	228.5	5.9	39.6	1.4	23.1
f) Nonnormalized 3-hr + ERBE clouds	228.5	7.1	42.5	2.5	27.8

(b) April 1985	NOAA-9 mean flux	Total error		Time interpolation error	
		Mean	rms	Mean	rms
Coincident data	251.0	5.1	39.1	-	-
Scaled coincident data	233.3	4.7	36.3	-	-
a) ERBE TSA	233.3	1.7	55.1	–3.0	41.4
b) w/ 1-hourly GOES + GOES clouds	233.3	5.7	37.1	1.0	7.5
c) w/ 3-hourly GOES + GOES clouds	233.3	3.4	38.5	–1.3	12.7
d) w/ 1-hourly GOES + ERBE clouds	233.3	5.2	39.9	0.4	16.5
e) w/ 3-hourly GOES + ERBE clouds	233.3	3.2	42.4	–1.5	21.8
f) Nonnormalized 3-hr + ERBE clouds	233.3	3.1	44.9	–1.6	26.4

relative effectiveness of the methods can be measured by comparing the rms errors. Thus, analysis of the simulations will stress a comparison of the instantaneous rms errors, not the biases.

The mean and rms errors due to time interpolation are calculated in a slightly different fashion than that used with the LW flux simulations. As can be seen in table 7.1-2, the mean SW flux for the coincident data is 20–30 W-m^{-2} greater than the mean fluxes used in the time interpolation. There are fewer (~7000) coincident data points as compared with the ~35000 NOAA-9 measurements that can be predicted from ERBS data. The difference in the mean fluxes occurs because these coincident data occur at a lower average solar zenith angle. To accommodate this difference, the rms errors from the coincident data (rms_o from equation 7.1-3) are first linearly scaled by the ratio of the mean fluxes before being subtracted from the total rms errors. These scaled values, which are used to calculate the time interpolation error, are shown in the second row of tables 7.1-2.

The addition of narrowband data into the process results in a significant decrease in the interpolation rms errors. As explained above, the ERBE time interpolation technique necessarily assumes constant cloudiness over each day for which there is only one time of observation. By introducing information concerning the temporal variation in cloudiness through the addition of narrowband data, the time interpolation error has been reduced from 43.1 W-m^{-2} to less than 28 W-m^{-2} in all cases (b)–(f) for the July data. The reasons for this increased accuracy can be seen in figure 7.1-4 which shows three days of SW albedo measured by ERBE during July 1985 in the same region as in figure 7.1-3. The ERBS observations are shown as black squares. The NOAA-9 observations are open circles. Also shown are the results of interpolations using the NOAA-9 data and the ERBE time interpolation technique (a) and the 3-hourly geostationary data technique (e). During the first two days, the cloudiness remained constant throughout the day and the two techniques produce similar results. On the third day, however, there was apparently a shift in cloudiness between the times of observation by ERBS and NOAA-9. The ERBE time interpolation technique severely overestimates the albedo over most of the day. The GOES data, however, provide the means for correctly modeling the albedo on that day.

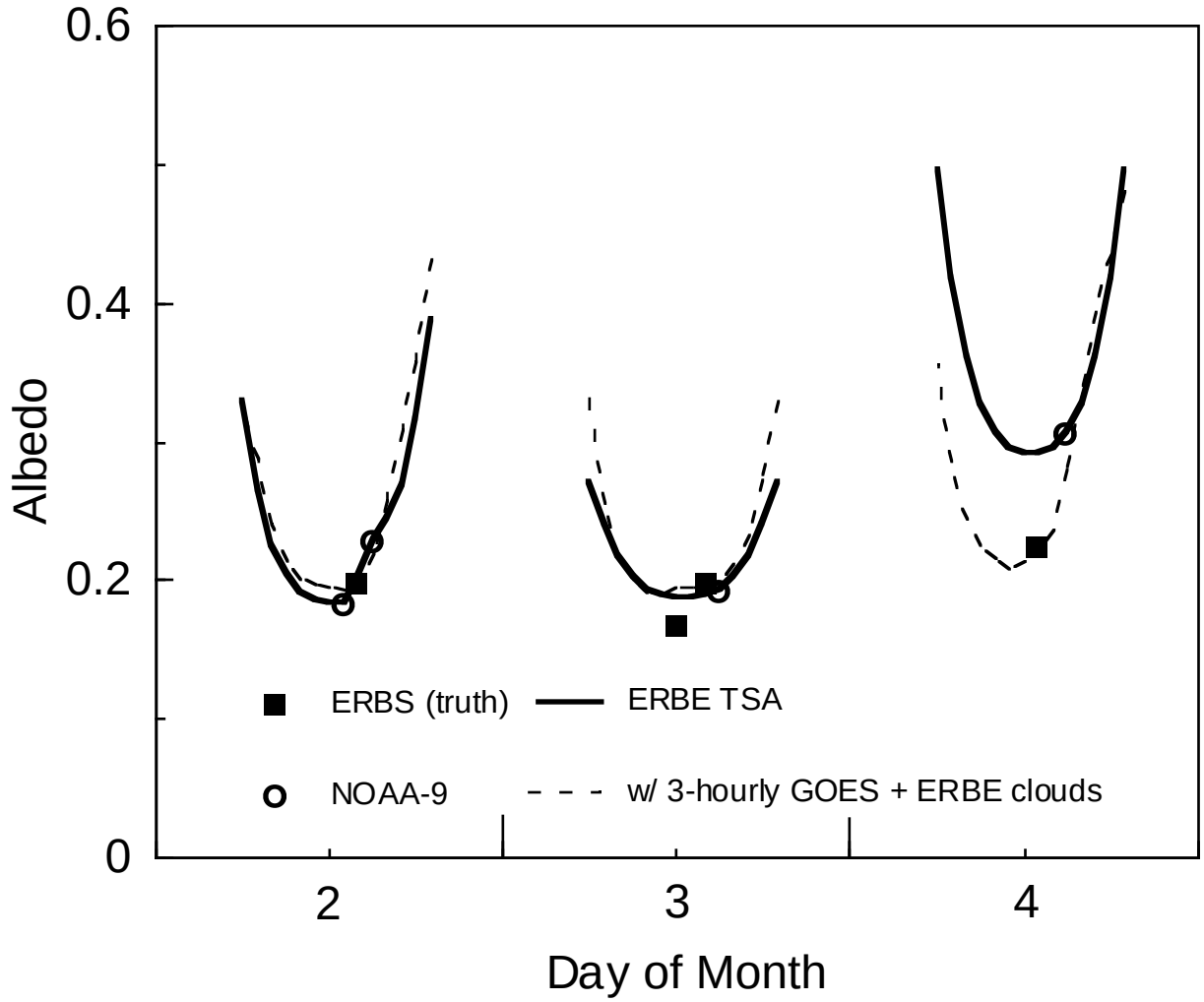

Figure 7.1-4. Time series of ERBE ERBS (■) and NOAA-9 (❍) SW albedo observations and interpolated values from July 1985 over New Mexico. The solid curve shows the ERBE time interpolated values; the dashed curve shows the geostationary-data-enhanced interpolation.

The technique currently proposed for release 2.1 is method (e). This method is a definite improvement over the ERBE technique, reducing the rms time interpolation error from 43.1 W-m^{-2} to 23.1 W-m^{-2} in July and from 41.4 W-m^{-2} to 21.8 W-m^{-2} in April. The bias errors also show improvement. As expected, the mean rms error associated with using 1-hourly data in method (d) shows a slight improvement over using 3-hourly data. However, this improvement is small compared to the advantages of data volume reduction if 3-hourly data are used instead. Furthermore, for generating SW flux estimates for synoptic maps, the difference between the 1-hourly and 3-hourly data is not significant. Since the fluxes will be derived at times of geostationary observations, the errors should be closer to the 1-hourly estimates shown here.

As is the case with LW flux data, the renormalization of the SW flux estimates to the nearest observation is important. The rms errors increase by 4–5 W-m^{-2} when this renormalization is not included in method (f).

An additional improvement is seen if cloud information is derived at the times of geostationary measurements. As stated above, errors from improper selection of SW ADM's can be quite large. Increasing the accuracy of cloud parameters should, therefore, decrease errors in the narrowband-

broadband conversion of the GOES data. For methods (d), (e), and (f), cloud fraction estimates are derived for each hour by linearly interpolating between ERBE observations. Cloud fractions derived directly from the narrowband data should be more accurate since time interpolation of cloud fraction is no longer necessary.

The results of using this improved cloud information are shown as methods (b) and (c) for 1-hourly and 3-hourly GOES data, respectively. For the 3-hourly case, rms interpolation errors decrease by 7–9 W-m^{-2} from method (e) which uses the ERBE cloud information. Part of this error is due to the linear interpolation of cloud fractions, but some of the error is due to incorrect ERBE scene identification. This latter error should be greatly diminished because of the improved cloud data from CERES. Thus, the improvement of method (c) over method (e) will not be as great for CERES. This method is not planned in release 2.1, but will be studied for possible addition to later releases.

These proposed changes in the temporal interpolation process are aimed at improving instantaneous estimates of flux. It is important to ensure that the estimates of monthly mean flux are not adversely affected. ERBE produced regional monthly mean SW flux estimates to within 3 W-m^{-2} (Harrison et al. 1990). For July, the ERBE method (a) produces monthly mean flux averaged over all regions of 95.1 W-m^{-2}. For methods (e) and (f), the averages are 95.5 W-m^{-2} and 95.6 W-m^{-2}, respectively. Thus, the enhancements to the interpolation process are not adversely affecting the monthly means. Once again, anchoring the SW fluxes to the observations in method (e) produces an improvement over the results of method (f).

From the results of these simulations, it is concluded that the introduction of geostationary data represents a significant improvement to the ERBE time interpolation technique, and will, therefore, be included into the CERES algorithm. The technique, method (e) will be used whenever narrowband data are available. The ERBE-like method (a) will be used for regions and times with no narrowband data.

7.1.2.8. Time interpolation of clear-sky TOA SW flux. As is the case with the clear-sky LW flux, there should be a more accurate assessment of the occurrence of clear-sky SW data with CERES than with ERBE. The CERES data are interpolated using the clear-sky ADM's appropriate to the regional surface type. The lack of geostationary data is not serious in the case of clear-sky modeling. The main information provided by the narrowband data is the changes in meteorology and cloudiness. For clear-skies, the CERES directional models should work well for time interpolation. Geostationary data could only be used in the processing of clear-sky data if cloud properties such as separate total-sky and clear-sky narrowband radiances are derived from the narrowband measurements. This is not planned for release 2.1. Simulations are underway to evaluate the relative merits of the two averaging methods for clear-sky parameters. If the ERBE-like method is sufficient, then method 2 time interpolation will not be performed for clear-sky SW.

7.1.2.9. Time interpolation of window radiances and surface-related parameters. The window channel interpolation should be straightforward. This measurement is made in the same spectral region as the infrared measurement from the geostationary satellites. Therefore, the geostationary LW radiance time series can be used in a manner similar to the technique employed to produce the time series of LW flux. The narrowband-broadband regressions will not be used, but the geostationary radiances will be normalized to the CERES measurements in order to correct for any differences in the spectral intervals or the calibration of the instruments.

Several parameters that describe surface characteristics will also be temporally interpolated to be used as input to the computation of atmospheric and surface fluxes. The surface emissivity and the surface scene type fraction array will be linearly interpolated since these should vary relatively slowly. The surface skin temperature is a more complicated problem. For release 2.1, the surface skin temperature will be interpolated in the same fashion as the clear-sky LW flux. For future releases, skin temperatures

from the MOA product may be used if available for the synoptic times, but these values may be normalized to the CERES observed values.

7.1.2.10. Algorithm core summary

7.1.2.10.1. Input data summary list. The chief input to the computation of synoptic maps is the gridded CERES SW and LW TOA fluxes and cloud information provided by the FSW data product. These data contain spatial averages of 1 hour of CERES measurements on a 1.0° equal-angle grid. The relevant parameters from FSW which are used in the averaging process are the total-sky LW and SW TOA fluxes, the clear-sky TOA LW and SW fluxes, and the CERES-derived cloud information. Geostationary satellite-derived radiances will be provided by the GEO data product. Additional data needed to perform this process include solar declination and the current ADM's. A detailed description of the input products is in appendix A.

7.1.2.10.2. Output data summary list. This process produces a global map of TOA total-sky LW and SW flux, TOA clear-sky LW and SW flux, TOA window radiances, and cloud parameters valid at 0, 3, 6, ..., 21 GMT for each day of the month. These synoptic results are used as inputs to computing synoptic maps of vertical radiation fields.

7.1.3. Implementation Issues for Temporal Interpolation

7.1.3.1. Strategic concerns. The major strategic concerns for this subsystem involve the accuracy and suitability of the method used for interpolating cloud properties. The methods used for the interpolation of TOA fluxes have been developed and tested with ERBE data. As demonstrated above, the linear assumption for cloud properties is acceptable when used to interpolate fluxes. However, the errors in the amount of cloud and its optical properties can cause significant errors in calculations of atmospheric and surface fluxes.

In order to assess the magnitude of this problem, a study of the instantaneous and monthly mean errors in cloud parameters such as cloud fraction and optical depth has been begun. As a truth set, one month of GOES one-hourly, 8-km data was analyzed on a 1.0-degree equal-angle grid over both the Tropical Ocean Global Atmosphere/Combined Ocean-Atmosphere Response Experiment (TOGA-COARE) region and the Oklahoma Atmospheric Radiation Measurement (ARM) central facility site using the Layer Bispectral Threshold Method (LBTM) technique of Minnis et al. (1995). For each region and hour, cloud properties including cloud fraction, optical depth, and cloud height were calculated for each of three levels of the atmosphere: high, mid, and low. The data were sampled to match the observational pattern of CERES TRMM, EOS-AM, and EOS-PM instruments. Cloud properties for the intervening times were interpolated using the CERES interpolation method described above. These interpolated values were then compared with the values from the truth set.

Cloud amount interpolation results for the TOGA-COARE region are compiled in Table 7.1-3. For the monthly mean cloud amount, the linear interpolation assumption produces reasonable values. The monthly mean cloud amount is within 4.3% of the true monthly means for all satellites. Greater errors occur for either EOS platform used by itself due to the lack of coverage of diurnal cloud variations.

Instantaneous errors are a greater concern. The rms errors in cloud amount are as high as 28.7% for the single-satellite case. In order to reduce these large errors, this data set has also been used to compute the gain in cloud interpolation accuracy that could be attained by the addition of cloud properties derived from the narrowband geostationary data at the synoptic times. The instantaneous errors in cloud fraction for TRMM can be reduced to 9.9%. The possibility of deriving these parameters in later releases is discussed in subsystem 11.0.

Errors in other cloud properties such as cloud height and optical depth are even greater due to the non-linear nature of clouds. Monthly mean optical depths rms errors are as high as 58% for single satellite cases. In addition, instantaneous errors are more difficult to estimate, particularly at times when only the interpolated or true cloud amount is non-zero. However, the ultimate goal of CERES temporal interpolation of clouds is not to produce monthly cloud products, but rather to provide input to the calculation of atmospheric and surface fluxes that are in balance with the CERES TOA fluxes. As explained in subsystem 5, the input cloud properties will be altered to obtain radiative balance. Therefore, a true measure of the impact of errors in cloud properties on the CERES synoptic product can only be obtained in future studies on the propagation of errors in the initial cloud property estimates through the calculation of the atmospheric and surface fluxes.

Table 7.1-3. Evaluation of CERES cloud amount time interpolation techniques. Results are for TOGA/COARE region for December, 1992. The truth cloud amount is 76.7%.

CERES Satellite Sampling Configuration	Mean value without GEO	Mean value with GEO	Relative RMS (%) without GEO (Instantaneous)	Relative RMS (%) with GEO (Instantaneous)	Relative RMS (%) without GEO (Monthly Mean)	Relative RMS (%) with GEO (Monthly Mean)
TRMM	73.6	76.6	28.7	9.9	5.3	0.4
TRMM+AM	72.5	76.6	26.3	9.6	5.7	0.4
TRMM+AM+PM	73.6	76.6	22.0	9.4	4.3	0.4

If cloud properties are derived at the synoptic times from geostationary data, they can be used to assist in the interpolation of clear-sky SW and LW fluxes. Geostationary radiances from areas classified as clear could be used to construct a clear-sky flux time series that could be normalized to CERES clear-sky measurements and applied in the same manner as the total-sky time series. This may be the greatest advantage in deriving geostationary cloud products. There may be large data gaps in the clear-sky flux records from CERES, as was the case with ERBE. The synoptic modeling process, however, requires a TOA clear-sky LW and SW flux at each synoptic time. Without the additional cloud information from the narrowband data, assumptions of persistence from the nearest day with data will have to be made. This is a greater problem in the LW than the SW, since the SW clear-sky albedo should not vary rapidly with time. The data gaps in both the clear-sky LW and SW will be handled in one of three ways:

1. The diurnal variation of clear-sky flux for days with no data will be modeled by interpolating between the diurnal curves of the two nearest days with data.
2. A monthly mean diurnal model will be constructed from days with data. This model will be applied to all days with no data.
3. The assumption of regional independence will be waived and clear data from surrounding regions with similar surface types will be used.

Studies are planned to assess the effects of clear-sky data gaps on the input to the synoptic radiative flux calculations.

Another consideration is the effect on derived cloud properties of increased viewing zenith angle. This effect has been noted by several authors (see Minnis 1989). Studies are being performed to determine if the error in interpolation increases when the viewing zenith angle of the geostationary data increases. If this is the case, then a viewing zenith angle limit may be imposed on these data.

Another aspect of the problem with data gaps is that decisions must be made concerning whether to restrict the time interval over which temporal interpolation is performed. ERBE interpolated TOA flux to all hours of the month if there was at least one observation during that month. For CERES, particularly for the synoptic product, there may be restrictions imposed based on simulation results. Since the rms errors of interpolation increase with the length of the time interval, at some point the error will

exceed acceptable limits. If such restrictions are incorporated, then flux estimates will not be made in regions without adequate time sampling. For release 2.1, data gaps of over 24 hours will not be filled with either LW of SW flux estimates.

The regressions that are to be used to produce broadband simulated fluxes from the narrowband measurements will have to be derived monthly. Separate, global regressions for ocean and land will be used initially. It has been demonstrated that for the simulations performed in this study, the effects of regional variations in these regressions can be minimized by the normalization of the LW and SW flux time series to the CERES measurements. If this normalization proves to be inadequate during the operational data analysis, then regional or climate-regime specific fits may be required each month using coincident CERES and geostationary data.

The simulations described above demonstrated that the linear interpolation of clouds does not seriously diminish the accuracy of the temporal interpolation of SW flux. However, since the clouds are linearly interpolated while the TOA fluxes include some information from the geostationary data concerning the changes in cloudiness, there will be instances when the clouds and TOA conditions will not be consistent. It is expected that most of this inconsistency will be removed during the recalculation of atmospheric fluxes. Several studies are planned to estimate the errors associated with this cloud property interpolation technique. Cloud properties derived from 1-hourly GOES data using the Hybrid Bispectral Threshold Method (Minnis et al. 1987) will be sampled and interpolated to calculate the errors.

All CERES gridded products will use the 1.0 equal-angle grid. Such a grid has increasingly smaller regions towards the poles that do not allow sufficient sampling of CERES footprints. In order to lessen this effect and to reduce the number of regions to process, spatial averaging and temporal interpolation may be performed on a modified, nested grid. This grid is described by Table 7.1-4. The advantage of this grid is twofold. First, the number of regions that need to be stored and processed decreased from 64800 to 44012. Second, regional sampling will be more uniform with latitude. The use of this grid will be strictly internal to the CERES processing system. The results of the larger “nested” regions will be reproduced for all 1.0 regions contained within it.

Table 7.1-4. Configuration of proposed CERES nested grid.

Latitude Range	Region Size	Total Regions
0 - 45	1 x 1	32400
45 -70	2 x 1	9000
70 - 80	4 x 1	1800
80 - 89	8 x 1	810
89 - 90	360 x 1	2
Total		44012

For release 2.1, the 12 ERBE LW and SW ADM’s will be used. CERES will create an extensive set of directional and bidirectional models that are applicable to specific combinations of cloud type, surface type, and possibly cloud optical depth which will be incorporated into release 4. The methods for including these models into the time interpolation process will be studied. For release 2.1, any updates to the ERBE ADMs that are incorporated in the reprocessing of the ERBE data will also be used for CERES.

The narrowband LW ADM used in equation 7.1-2 was developed by Minnis et al. (1991) using theoretical calculations and is scene ID independent. New, expanded narrowband ADM’s may be developed. Additionally, the simulations will be performed using the ERBE broadband ADM’s in place of the narrowband model. If no degradation in the results occurs, the ERBE ADM’s will be used.

7.1.3.2. Scientific implementation issues

7.1.3.2.1. Calibration. There are two primary calibration considerations for this subsystem. The first is the narrowband-broadband correlations for both SW and LW. This was addressed above in section 7.1.3.1. The second consideration is the calibration of the narrowband radiances for each of the geostationary satellites. If the data source for these data is the ISCCP, the data will have already been calibrated. If the data are not previously calibrated, then procedures will be developed for this purpose. However, the proposed averaging method incorporates safeguards to properly account for both long-term drifts and shorter time scale variations in instrument calibration. Long-term variations in the stability of the geostationary sensors will not present problems to the averaging process since the narrowband-broadband correlations used during the averaging will be recomputed for each sensor for each month of data. Shorter-term variations (of less than 1 month) will also be largely eliminated by the continuous renormalization of the simulated broadband data to the closest CERES observation.

7.1.3.2.2. Validation. In addition to the previously discussed ongoing efforts to test the time-interpolated data, several validation studies are planned to determine the uncertainties in the interpolated cloud properties and surface and TOA fluxes. The new series of the GOES satellites will have 4-km resolution data available every half hour at wavelengths comparable to the VIRS and the Advanced Very High Resolution Radiometer (AVHRR). The CERES cloud analysis algorithms will be applied to selected intervals of data taken by the new GOES to derive a high temporal resolution data set of cloud properties and narrowband-based fluxes. Sampling studies using the time interpolation algorithms will be conducted using the GOES results as the reference case. These validation efforts will be used to quantify the errors introduced in the time interpolation process and to develop improved techniques.

Other validation studies will utilize long-term data sets taken during field programs. The Atmospheric Radiation Measurement (ARM) project plans to measure the surface radiation budget continuously at a minimum of three locations including sites in the central U.S., the tropical Pacific, and the Arctic. The temporal and spatial scales of these instrumented sites are compatible with the CERES regional grid. Unmanned Aerospace Vehicles (UAV's) are also planned as part of ARM. The basic instrument package includes both broadband longwave and shortwave flux radiometers. The UAV's are capable of flying at stratospheric altitudes during missions lasting up to a week. They can be programmed to cover areas as large as the CERES regions. These platforms provide an ideal, calibrated source to validate the time interpolation results over limited but significantly different areas. Other instruments on these UAV's may be used to derive coincident cloud properties. Other field programs including the First ISCCP Regional Experiment (FIRE), SHEBA, and components of the Global Energy and Water Cycle Experiment (GEWEX) may also provide high-temporal resolution data sets that can be used to validate the CERES products.

The CERES Validation Plans are currently being developed. Following a peer review in late 1996, the Validation Plans will be made available on the WWW in the Spring of 1997. In the interim, a separate document containing the Validation Plan Summary Charts for each major subsystem has been developed to accompany these ATBDs.

7.2. Compute Surface and Atmospheric Fluxes at Synoptic Times

The CERES Data Management System calculates the full column of the SARB at synoptic times. This process produces a set of archival radiative fluxes at the surface, TOA, and at various atmospheric levels. The SARB calculations are based on the cloud and meteorological inputs that have been interpolated to synoptic times. The radiation calculated at the TOA is compared to the TOA fluxes that are generated at synoptic times as described in section 7.1. If necessary, the cloud and meteorological parameters that are used as inputs to the radiation calculations are tuned, as in subsystem 5, to balance

the satellite-based synoptic TOA fluxes. This tuning process produces a set of adjustments to the synoptic cloud and meteorological data, as well as the SARB at synoptic times.

Because this section so closely follows subsystem 5, which describes the SARB calculations and the tuning of the cloud and meteorological variables at the instantaneous ERBE or CERES footprint scale, this section has been kept brief. Subsystem 5 contains a more detailed treatment and a scientific discussion.

7.2.1. Synoptic Data for Input to Radiative Transfer Calculations

The cloud, meteorological, and TOA fluxes which have been estimated for synoptic times by process 7.1 are used to calculate the radiative fluxes through the atmospheric column. The Release 2 algorithm for the calculation of these fluxes is analogous to the algorithm in section 5.3.

The meteorological input is based on an NWP-analyzed (DAO and/or NCEP) sounding and is interpolated into the combination of fixed and floating vertical levels (maximum number 34; shown in Fig. 8 of the section 5.3) in the CERES horizontal grid. Cloud properties available for the calculation are described in Table 4 of section 5.3.2.1. For up to four distinct pressure categories (low, lower middle, upper middle, and high), we use the mean cloud areas, cloud effective temperature, cloud particle size and phase, and the logarithmic mean visible optical depth. Section 7.1.2.4 describes the interpolation of the cloud properties derived from the CERES cloud imager retrievals using cloud area weighting for all cloud properties in the pressure categories. The initial surface albedo is interpolated from the CERES retrievals, with an adjustment for solar zenith angle.

7.2.2. Initial Calculation of Synoptic Radiative Fluxes

Subsystem 5 describes the SARB retrieval algorithm, which uses the delta-4-stream, correlated-k Fu and Liou (1993) radiative transfer code. The algorithm is used to calculate clear-sky TOA fluxes (this is computed and archived, even if the region is overcast) and TOA fluxes for each of the synoptic cloud conditions. These initial, untuned radiative transfer calculations are archived at only the surface and TOA for (1) clear-sky and (2) the estimated total-sky condition for the region.

After the initial clear-sky and total-sky calculations are performed, the TOA total-sky calculated results for the region are compared to the CERES averages. A tuning, or constrainment, is then conducted as described in section 5.3.3. Candidate variables are adjusted to bring the computed fluxes into agreement with the observed fluxes, to within specified uncertainties. The variables which are adjusted include the surface skin temperature, the precipitable water, the surface albedo, the cloud liquid water path (LWP; which scales into visible optical depth), the cloud top temperature, the aerosol optical depth, and the cloud fraction. Radiative transfer calculations are again performed with the adjusted variables. Tuned fluxes are saved at the surface, 500 hPa, the tropopause, and TOA for clear-sky and total-sky conditions.

7.2.3. Strategic Concerns

Subsystem 5 contains scientific discussion of problems relating to the calculation of the SARB, and strategic concerns are highlighted in section 5.5. One outstanding concern for the production of fluxes and adjusted cloud and meteorological data at synoptic times, is the limitation posed in the synoptic calculations at the large scale of the CERES grid boxes. In subsystem 5, the calculations are performed at the smaller scale of each ERB footprint (FOV). The averaging of input data or calculations introduces error. An opportunity exists to investigate the errors at this scale, by studies with the CRS (subsystem 5) and FSW (subsystem 6) outputs from the pre-launch Release 1. CRS contains clouds and calculated radiative fluxes at the CERES FOV. Those footprint scale cloud properties can be averaged in FSW with the same assumptions used to generate synoptic clouds and fluxes. By performing a synoptic-like calculation with the hourly data in the FSW grid, results can be compared with the standard FSW clouds

and fluxes, to learn if a bias is introduced by the synoptic-like spatial averaging process itself. Limited calculations thus far find only a small bias.

A second strategic concern, particular to the synoptic flux calculations, is the accuracy of the temporal interpolation. A small scale, but spatially intensive data set of sounding, cloud property, and calculated and observed fluxes has been developed to investigate this. The CERES/ARM/GEWEX Experiment (CAGEX) is an on-line resource now covering April 5-30, 1994; daylight only; half hourly GOES data and calculations; 3x3 grid at the ARM CART SGP site in Oklahoma (http://snow-dog.larc.nasa.gov:/cagex.html). An interpolation study is planned with CAGEX.

The CERES SARB calculations will be performed on a 3-hourly basis for the synoptic flux computation. Raw averages of 3-hourly fluxes are not adequate for determining the daily mean SW fluxes at the surface and within the atmosphere because of the diurnal course of the Sun. Algorithms for mapping the 3-hourly synoptic fluxes to astronomically consistent daily averaged surface and atmospheric fluxes will be developed using temporally intensive calculations.

7.3. References

Barkstrom, B. R. 1984: The Earth Radiation Budget Experiment (ERBE). *Bull. American Meteorol. Soc.,* vol. 65, pp. 1170–1185.

Barkstrom, Bruce R.; Harrison, Edwin F.; and Lee, Robert B., III 1990: Earth Radiation Budget Experiment—Preliminary Seasonal Results. *EOS*, vol. 71, pp. 279, 299, 304, and 305.

Barkstrom, B. R.; and Smith, G. L. 1986: The Earth Radiation Budget Experiment—Science and Implementation. *Rev. Geophys.*, vol. 24, pp. 379–390.

Briegleb, B.; and Ramanathan, V. 1982: Spectral and Diurnal Variations in Clear Sky Planetary Albedo. *J. Appl. Meteorol.*, vol. 21, pp. 1160–1171.

Brooks, D. R.; and Minnis, P. 1984: Simulation of the Earth's Monthly Average Regional Radiation Balance Derived From Satellite Measurements. *J. Climat. & Appl. Meteorol*., vol. 23, pp. 392–403.

Brooks, D. R.; Harrison, E. F.; Minnis, P.; Suttles, J. T.; and Kandel, R. S. 1986: Development of Algorithms for Understanding the Temporal and Spatial Variability of the Earth's Radiation Balance. *Rev. Geophys.*, vol. 24, pp. 422–438.

Desbois, Michel; Kayiranga, Theoneste; and Gnamien, Brigitte 1989: Diurnal Cycle of Convective Cloudiness Over Tropical Africa Observed From Meteosat—Geographic Characterization and Interannual Variations. *Annales Geophys.*, vol. 7, pp. 395–404.

Doelling, David R.; Young, David F.; Arduini, Robert F.; Minnis, Patrick; Harrison, Edwin F.; and Suttles, J. T. 1990: On the Role of Satellite-Measured Narrowband Radiances for Computing the Earth's Radiation Balance. *Seventh Conference on Atmospheric Radiation—Preprints*, American Meteorol. Soc., pp. 155–160.

Garand, Louis 1988: Automated Recognition of Oceanic Cloud Patterns. I—Methodology and Application to Cloud Climatology. *J. Climat*., vol. 1, pp. 20–39.

Harrison, E. F.; Young, D. F.; Minnis, P.; Wielicki, B. A.; Doelling, D. R.; and Gibson, G. G. 1994: Temporal Sampling Analysis for the Clouds and the Earth's Radiant Energy System (CERES) Experiment for Satellite Missions in the Late 1990's. *Seventh Conference on Satellite Meteorology and Oceanography*, pp. 520–523.

Harrison, Edwin F.; Brooks, David R.; Minnis, Patrick; Wielicki, Bruce A.; and Staylor, W. Frank 1988: First Estimates of the Diurnal Variation of Longwave Radiation From the Multiple-Satellite Earth Radiation Budget Experiment (ERBE). *Bull. American Meteorol. Soc.*, vol. 69, pp. 1144–1151.

Harrison, E. F.; Minnis, P.; Barkstrom, B. R.; Ramanathan, V.; and Cess, R. D. 1992: Seasonal Variation of Cloud Radiative Forcing Derived From the Earth Radiation Budget Experiment. *J. Geophys. Res.*, vol. 95, pp. 18687–18703.

Minnis, Patrick 1989: Viewing Zenith Angle Dependence of Cloudiness Determined From Coincident GOES East and GOES West Data. *J. Geophys. Res*., vol. 94, pp. 2303–2320.

Minnis, P.; and Harrison, E. F. 1984: Diurnal Variability of Regional Cloud and Clear-Sky Radiative Parameters Derived From GOES Data. III—November 1978 Radiative Parameters. *J. Climat. & Appl. Meteorol.*, vol. 23, pp. 1033–1051.

Minnis, Patrick; Harrison, Edwin F.; and Gibson, Gary G. 1987: Cloud Cover Over the Equatorial Eastern Pacific Derived From July 1983 International Satellite Cloud Climatology Project Data Using a Hybrid Bispectral Threshold Method. *J. Geophys. Res.*, vol. 92, pp. 4051–4073.

Minnis, Patrick; Harrison, Edwin F.; and Young, David F. 1991: Examination of the Relationship Between Outgoing Infrared Window and Total Longwave Fluxes Using Satellite Data. *J. Climat.*, vol. 4, pp. 1114–1133.

Minnis, P.; Smith, Jr., W. L.; Garber, D. P.; Ayers, J. K.; and Doelling, D.R. 1995: *Cloud Properties Derived From GOES-7 for the Spring 1994 ARM Intensive Observing Period Using Version 1.0.0 of the ARM Satellite Data Analysis Program*. NASA RP-1366.

Minnis, P.; Takano, Y.; and Liou, K.-N. 1993: Inference of Cirrus Cloud Properties Using Satellite-Observed Visible and Infrared Radiances, Part I: Parameterization of Radiance Fields. *J. Atmos. Sci.*, vol. 50, pp. 1279-1304.

Suttles, J. T.; Green, R. N.; Minnis, P.; Smith, G. L.; Staylor, W. F.; Wielicki, B. A.; Walker, I. J.; Young, D. F.; Taylor, V. R.; and Stowe, L. L. 1988: *Angular Radiation Models for Earth-Atmosphere System. Volume 1—Shortwave Radiation.* NASA RP-1184.

Suttles, J. T.; Green, R. N.; Smith, G. L.; Wielicki, B. A.; Walker, I. J.; Taylor, V. R.; and Stowe, L. L. 1988: *Angular Radiation Models for Earth-Atmosphere System. Volume 2—Longwave Radiation*. NASA RP-1184.

Wielicki, Bruce A.; and Barkstrom, Bruce R. 1991: Clouds and the Earth's Radiant Energy System (CERES)—An Earth Observing system Experiment. S*econd Symposium on Global Change Studies—Preprints*, American Meteorol. Soc., pp. 11–16.

Appendix A

Input Data Products

Merge Satellites, Time Interpolate, Compute Fluxes (Subsystem 7.0)

This appendix describes the data products which are used by the algorithms in this subsystem. Table A-1 below summarizes these products, listing the CERES and EOSDIS product codes or abbreviations, a short product name, the product type, the production frequency, and volume estimates for each individual product as well as a complete data month of production. The product types are defined as follows:

Archival products:	Assumed to be permanently stored by EOSDIS
Internal products:	Temporary storage by EOSDIS (days to years)
Ancillary products:	Non-CERES data needed to interpret measurements

The following pages describe each product. An introductory page provides an overall description of the product and specifies the temporal and spatial coverage. The table which follows the introductory page briefly describes every parameter which is contained in the product. Each product may be thought of as metadata followed by data records. The metadata (or header data) is not well-defined yet and is included mainly as a placeholder. The description of parameters which are present in each data record includes parameter number (a unique number for each distinct parameter), units, dynamic range, the number of elements per record, an estimate of the number of bits required to represent each parameter, and an element number (a unique number for each instance of every parameter). A summary at the bottom of each table shows the current estimated sizes of metadata, each data record, and the total data product. A more detailed description of each data product will be contained in a user's guide to be published before the first CERES launch.

Table A-1. Input Products Summary

Product code		Name	Type	Frequency	Size, MB	Monthly size, MB
CERES	EOSDIS					
MOA	CERX06	Meteorological, Ozone, and Aerosol Data	Archival	1/Hour	11.55	8591
GGEO	CERX14	Grid Geostationary Narrowband Radiances	interim	1/month	816.1	816.1
FSW	CER05	Gridded Single Satellite Fluxes and Clouds	Archival	1/Month	69.5	12511.8

Meteorological, Ozone, and Aerosol Data (MOA)

The CERES archival product Meteorological, Ozone, and Aerosol Data (MOA) is produced by the CERES Regrid MOA Subsystem. Each MOA file contains meteorological, ozone, and aerosol data for one hour, and is used by several of the CERES subsystems. Data on the MOA are derived from several data sources external to the CERES system, such as the Data Assimilation Office (DAO), NOAA, and various other meteorological satellites. These data arrive anywhere from four times daily to once a month, and have various horizontal resolutions. The Regrid MOA Subsystem interpolates the aerosol and ozone data horizontally to conform with the horizontal resolution of the meteorological data. Profile data are interpolated vertically to conform with CERES requirements. All data are temporally interpolated to provide data to the CERES processing system on an hourly basis.

The MOA contains:

- Surface pressure, geopotential height, skin temperature, and sea surface state
- Vertical profiles of temperature and humidity for 58 atmospheric levels

- Vertical profiles for 18 atmospheric levels below the tropopause of wind u-vector and v-vector data
- Tropospheric height
- Air mass index
- Column precipitable water based on humidity profiles
- Column precipitable water based on microwave measurements
- Column averaged relative humidity
- Vertical profile of ozone mixing ratios for 58 atmospheric levels
- Column ozone
- Aerosol optical depth

Level: 3
Type: Archival
Frequency: 1/Hour

Portion of Globe Covered
File: Global
Record: One region

Time Interval Covered
File: 1 hour
Record: 1 hour

Portion of Atmosphere Covered
File: Surface to TOA

Table A-2. Meteorological, Ozone, and Aerosol (MOA)

Description	Parameter Number	Units	Range	Elements/ Record	Bits/ Elem	Elem Num
Header						
Date and Hour		N/A	ASCII string	1	216	
MOA Processing Date		N/A	ASCII string	1	216	
MOA Grid Index		N/A	1 .. 1	1	16	
Number of MOA Regions		N/A	13104 .. 13104	1	32	
Temperature, Humidity, and Ozone Profile Fixed Pressure Levels		hPa	0 .. 1100	55	32	
Wind Speed Profile Pressure levels		hPa	0 .. 1100	18	32	
Surface Data						
MOA Region Number	1	N/A	1 .. 13104	1	32	1
Surface Pressure	2	hPa	0 .. 1100	1	32	2
Surface Geopotential Height	3	m	-100 .. 10000	1	32	3
Surface Skin Temperature	4	K	175 .. 375	1	32	4
Flag, Sea Surface State	5	N/A	0 .. 9	1	32	5
Flag, Source Surface Data	6	N/A	TBD	1	32	6
Meteorological Profiles						
Temperature Profiles	7	K	175 .. 375	58	32	7
Specific Humidity Profiles	8	N/A	0 .. 100	58	32	65
Wind Profile, U-Vector	9	m sec^{-1}	-100 .. 100	18	32	123
Wind Profile, V-Vector	10	m sec^{-1}	-100 .. 100	18	32	141
Flag, Source Meteorological Profiles	11	N/A	TBD	1	32	159
Meteorological Column Data						
Tropospheric Height	12	hPa	150 .. 300	1	32	160
Air Mass Index	13	N/A	0 .. 10	1	32	161
Precipitable Water	14	cm	0.001 .. 10.000	1	32	162
Column Averaged Relative Humidity	15	N/A	0 .. 100	1	32	163
Microwave Precipitable Water	16	cm	0.001 .. 10.000	1	32	164
Microwave Precipitable Water, std	17	cm	TBD	1	32	165
Flag, Source Microwave Column Precipitable Water	18	N/A	TBD	1	32	166
Ozone Profile Data						
Ozone Mixing Ratio Profiles	19	g kg^{-1}	0.00002 .. 0.02	58	32	167
Flag, Source Ozone Profile Data	20	N/A	TBD	1	32	225
Column Ozone						
Column Ozone	21	du	0 .. 500	1	32	226
Flag, Source Column Ozone	22	N/A	TBD	1	32	227
Total Column Aerosol						
Optical Depth, Total Column	23	g m^{-2}	0 .. 2	1	32	228
Flag, Source Optical Depth, Total Column	24	N/A	TBD	1	32	229
Spares	25	N/A	TBD	2	32	230

Total Header Bits/File:	544
Total Data Bits/Record:	7392
Total Records/File:	13104
Total Data Bits/File:	96864768
Total Bits/File:	96865312

Gridded Geostationary Narrowband Radiances (GGEO)

The GGEO product is a single file containing a header record followed by multiple data records. The header record contains information to identify the product contents and version. These data are the CERES Data Product Code, the Data Starting and Ending Date, and the Product Creation Date and Time.

Each data record, called an hourbox, contains data particular to a single grid region and hour. The number of hourboxes on the file is constant and is determined by the number of data hours per day, the maximum number of days per month, and the number of regions in the grid (8 hours per day x 31 days per month x 64800 regions on globe = 16,070,400 hourboxes). Hourboxes for which there are no ISCCP data are filled with default values.

The data record (hourbox) contains 3 categories of data: Satellite and Hourbox ID information, Key Footprint Parameters, and Radiance Statistics.

- The **Satellite and Hourbox ID** information, as the name implies, identifies the hourbox, as well as the satellite which collected the data within the hourbox. Although there are many grid regions on the earth that are observed by more than one geostationary satellite, each hourbox contains only data from the closest observing satellite.
- The **Key Footprint Parameters** are data associated with the key footprint, the footprint which falls closest to the centroid of the region. These data are the time of the footprint and three angle measurements associated with the footprint: the cosine of the satellite zenith angle, the cosine of the solar zenith angle, and the relative azimuth angle.
- The primary data on the GGEO product are **Radiance Statistics**. These are visible and infrared radiance values averaged over a grid region every 3rd hour of each month. The statistics contain, in order, the calculated mean and variance, and the number of footprints used for the calculations.

Level: 3
Type: Ancillary
Frequency: Monthly

Portion of Globe Covered
File: Entire globe
Record: 1.0 degree equal angle regions

Time Interval Covered
File: Monthly
Record: Every third hour

Portion of Atmosphere Covered
File: TOA

Table A-3. Gridded Geostationary Narrowband Radiances (GGEO)

Description	Parameter Num	Unit	Range	Elements/ Record	Bits/ Elem	Elem Num	Bits/ Rec
GGEO							
GGEO Header							
CERES Data Product Code		N/A	N/A	1	32		32
Data Starting Date		N/A	N/A	1	32		32
Data Ending Date		N/A	N/A	1	32		32
Product Creation Date		N/A	N/A	1	32		32
Product Creation Time		N/A	N/A	1	32		32
GGEO Record							
Satellite and Hourbox ID							
Satellite Number	1	N/A	N/A	1	32	1	32
Region Number	2	N/A	1 .. 64800	1	32	2	32
Hour Number	3	N/A	1 .. 744	1	32	3	32
Key Footprint Parameters							
Time	4	hhmmss	0 .. 235959	1	32	4	32
Cos of Satellite Zenith Angle	5	N/A	-1.0 .. 1.0	1	32	5	32
Cos of Solar Zenith Angle	6	N/A	-1.0 .. 1.0	1	32	6	32
Relative Azimuth Angle	7	Degrees	0.0 .. 180.0	1	32	7	32
Radiance Statistics							
visible radiance: mean, var, num obs	8	$W/m^2/SR$	0.0 .. 20.0	3	32	8	96
infrared radiance: mean, var, num obs	9	$W/m^2/\mu m/SR$	0.0 .. 600.0	3	32	11	96

Total Meta Bits/File:	160
Total Data Bits/Record:	416
Total Records/File:	16070400
Total Data Bits/File:	6685286400
Total Bits/File:	6685286560
Total Data Bytes/Record:	52
Total Data Bytes/File	835660800
Total Files/Product:	1

Grid Single Satellite Fluxes and Clouds (FSW)

The Monthly Gridded Single Satellite Fluxes and Clouds (FSW) archival data product contains hourly single satellite flux and cloud parameters averaged over 1.0 degree regions. Input to the FSW Subsystem is the Single Satellite CERES Footprint, Radiative Fluxes and Clouds (CRS) archival data product. Each FSW covers a single month swath from a single CERES instrument mounted on one satellite. The product has a product header and multiple records; each record contains spatially averaged data for an individual region.

The major categories of data output on the FSW are as follows:

- Region data
- Total-sky radiative fluxes at TOA, surface, and atmospheric levels
- Clear-sky radiative fluxes at TOA, surface, and atmospheric levels
- Cloud overlap conditions
- Cloud category properties
- Column-averaged cloud properties
- Angular model scene classes
- Surface-only data
- Adjustment parameters

FSW is an archival product generated on an monthly basis. Initially, at the launch of the TRMM spacecraft, this product will be produced in validation mode once every 3 months, or for 4 data months a year. During the first 18 months after the launch of TRMM, the CERES Science Team will derive a production quality set of ADMs, which are needed to produce the SW and LW instantaneous fluxes. Eighteen months after the launch of TRMM, this product will be archived and will contain SW and LW fluxes at the tropopause and at the 500 hPa pressure level, in addition to fluxes at TOA and at the surface. Thirty-six months after the launch of TRMM, this archived product will contain SW and LW fluxes at 26 standard pressure levels. A complete listing of parameters for this data product can be found in Table .

Level: 3
Type: Archival
Frequency: 1/Month

Time Interval Covered
File: Month
Record: Hour

Portion of Globe Covered
File: Gridded satellite swath
Record: 1.0-degree equal-angle regions

Portion of Atmosphere Covered
File: TOA, surface, and atmospheric pressure levels

Table A-4. Monthly Gridded Single Satellite Fluxes and Clouds (FSW)

Description	Parameter Num	Unit	Range	Elements/ Record	Bits/ Elem	Elem Num
FSW Header						
CERES Data Product Code		N/A	N/A	1	32	
CERES Spacecraft Identification Code		N/A	N/A	1	32	
CERES Instrument Identification code		N/A	N/A	1	32	
Zone Number		N/A	1 .. 180	1	32	
Data Year		N/A	1996 .. 2099	1	32	
Data Month		N/A	1 .. 12	1	32	
Number of hours per region		N/A	0 .. 744	360	32	
Data Date Processed		N/A	N/A	1	136	
FSW Record						
Description	**Parameter Num**	**Unit**	**Range**	**Elements/ Record**	**Bits/ Elem**	**Elem Num**
Spatially Averaged Region Parameters						
Time and Position Data						
Key Footprint Parameters						
Julian Time	1	Day	0.0 .. 1.0	1	32	1
Sun colatitude	2	Degrees	0.0 .. 180.0	1	32	2
Sun longitude	3	Degrees	0.0 .. 360.0	1	32	3
Relative azimuth angle at TOA	4	Degrees	0.0 .. 360.0	1	32	4
Cosine of solar zenith angle at TOA	5	N/A	0.0 .. 1.0	1	32	5
Spacecraft zenith angle	6	Degrees	0.0 .. 90.0	1	32	6
Region ID						
Region number	7	Dimensionless	1 .. 64800	1	32	7
Hour box number	8	Dimensionless	1 .. 744	1	32	8
Number of Footprints in region	9	N/A	1 .. 40	1	32	9
Number of imager pixels in CERES fov in the region	10	N/A	1 .. 360000	1	32	10
Other Regional Parameters						
Altitude of surface above sea level	11	m	-1000 .. 10000	1	32	11
Surface type percentage: mean	12	Percent	0.0 .. 100.0	20	32	12
Sunglint percent coverage	13	Percent	0.0 .. 100.0	1	32	32
Snow/Ice percent coverage	14	Percent	0.0 .. 100.0	1	32	33
Smoke percent coverage	15	Percent	0.0 .. 100.0	1	32	34
Fire percent coverage	16	Percent	0.0 .. 100.0	1	32	35
Imager radiance, clear-sky area	17	W $m^{-2}sr^{-1}um^{-1}$	TBD	5	32	36
Total aerosol visible optical depth, clear-sky area	18	N/A	0.0 .. 2.0	1	32	41
Total aerosol effective radius, clear-sky area	19	um	0.0 .. 20.0	1	32	42
Imager percent coverage	20	Percent	0.0 .. 100.0	1	32	43
Precipitable Water	21	cm	0.0001 .. 10.0	1	32	44
Shadowed pixels percent coverage (TBD)	22	Percent	0.0 .. 100.0	1	32	45
Imager viewing zenith angle over CERES FOV	23	Degrees	0.0 .. 90.0	1	32	46
Imager relative azimuth angle over CERES FOV	24	Degrees	0.0 .. 360.0	1	32	47
Imager channel identifier	25	N/A	1 .. 20	5	32	48
Imager radiance over CERES FOV, 5th percentile	26	W $m^{-2}sr^{-1}um^{-1}$	TBD	5	32	53
Imager radiance over CERES FOV	27	W $m^{-2}sr^{-1}um^{-1}$	TBD	5	32	58
Imager radiance over CERES FOV, 95th percentile	28	W $m^{-2}sr^{-1}um^{-1}$	TBD	5	32	63
Spatially Averaged Radiative Flux Parameters						
TOA Clear-Sky Fluxes is Array[3] of:						
Upward SW flux at TOA: mean, std, num obs	29	W m^{-2}	0.0 .. 1400.0	3	32	68
Upward LW flux at TOA: mean, std, num obs	30	W m^{-2}	100.0 .. 500.0	3	32	71
Upward LW window flux at TOA: mean, std, num obs	31	W m^{-2}	0.0 .. 800.0	3	32	74
Albedo: mean, std, num obs	32	Dimensionless	0.0 .. 1.0	3	32	77
TOA Total-Sky Fluxes is Array[3] of:						
Upward SW flux at TOA: mean, std, num obs	33	W m^{-2}	0.0 .. 1400.0	3	32	80
Upward LW flux at TOA: mean, std, num obs	34	W m^{-2}	100.0 .. 500.0	3	32	83
Upward LW window flux at TOA: mean, std, num obs	35	W m^{-2}	0.0 .. 800.0	3	32	86
Albedo: mean, std, num obs	36	Dimensionless	0.0 .. 1.0	3	32	89
Atmospheric Clear-Sky Flux Profiles for 4 Layers (Layers: sfc, 500hPa, tropopause, and TOA AVG) is Array[3] of:						
Downward SW flux, Model A: mean, std, num obs	37	W m^{-2}	0.0 .. 1400.0	12	32	92
Upward SW flux: mean, std, num obs	38	W m^{-2}	0.0 .. 1400.0	12	32	104
Downward LW flux, Model A: mean, std, num obs	39	W m^{-2}	0.0 .. 500.0	12	32	116
Upward LW flux: mean, std, num obs	40	W m^{-2}	0.0 .. 500.0	12	32	128

Description	Parameter Num	Unit	Range	Elements/ Record	Bits/ Elem	Elem Num
Atmospheric Total-Sky Flux Profiles for 4 Layers						
(Layers: sfc, 500hPa, tropopause, and TOA AVG) is Array[3] of:						
Downward SW flux, Model A: mean, std, num obs	41	W m^{-2}	0.0 .. 1400.0	12	32	140
Upward SW flux: mean, std, num obs	42	W m^{-2}	0.0 .. 1400.0	12	32	152
Downward LW flux, Model A: mean, std, num obs	43	W m^{-2}	0.0 .. 500.0	12	32	164
Upward LW flux: mean, std, num obs	44	W m^{-2}	0.0 .. 500.0	12	32	176
Clear-Sky Flux_Adjustments (Tuned-Untuned) is Array[3] of:						
Surface Layer:						
Downward SW flux: mean, std, num obs	45	W m^{-2}	0.0 .. 1400.0	3	32	188
Upward SW flux: mean, std, num obs	46	W m^{-2}	0.0 .. 1400.0	3	32	191
Downward LW flux: mean, std, num obs	47	W m^{-2}	0.0 .. 500.0	3	32	194
Upward LW flux: mean, std, num obs	48	W m^{-2}	0.0 .. 500.0	3	32	197
TOA Layer:						
Upward Sw flux: mean, std, num obs	49	W m^{-2}	0.0 .. 1400.0	3	32	200
Downward LW flux: mean, std, num obs	50	W m^{-2}	0.0 .. 500.0	3	32	203
Upward LW flux: mean, std, num obs	51	W m^{-2}	0.0 .. 500.0	3	32	206
Total-Sky Flux_Adjustments (Tuned-Untuned) is Array[3] of:						
Surface Layer:						
Downward SW flux: mean, std, num obs	52	W m^{-2}	0.0 .. 1400.0	3	32	209
Upward SW flux: mean, std, num obs	53	W m^{-2}	0.0 .. 1400.0	3	32	212
Downward LW flux: mean, std, num obs	54	W m^{-2}	0.0 .. 500.0	3	32	215
Upward LW flux: mean, std, num obs	55	W m^{-2}	0.0 .. 500.0	3	32	218
TOA Layer:						
Upward Sw flux: mean, std, num obs	56	W m^{-2}	0.0 .. 1400.0	3	32	221
Downward LW flux: mean, std, num obs	57	W m^{-2}	0.0 .. 500.0	3	32	224
Upward LW flux: mean, std, num obs	58	W m^{-2}	0.0 .. 500.0	3	32	227
Emissivity						
LW surface emissivity	59	N/A	0 .. 1	1	32	230
WN surface emissivity	60	N/A	0 .. 1	1	32	231
Surface Only Data						
Photosynthetically active radiation	61	W m^{-2}	0.0 .. 780.0	1	32	232
Direct/Diffuse	62	N/A	0.0 .. 30.0	1	32	233
Spatially Averaged Cloud Parameters						
Spatially Averaged Cloud Overlap Conditions						
Overlap condition weighted area percentage	63	Percent	0.0 .. 100.0	11	32	234
Spatially Averaged Cloud Category Data for 4 Layers						
(High, Upper Middle, Lower Middle, and Low)						
Spatially Averaged Cloud Area Fractions						
Overcast percent coverage	64	Percent	0.0 .. 100.0	4	32	245
Total percent coverage	65	Percent	0.0 .. 100.0	4	32	249
Spatially Averaged Cloud Properties is Array[3] of:						
Cloud effective pressure: mean, std, num obs	66	hPa	0.0 .. 1100.0	12	32	253
Cloud effective temperature: mean, std, num obs	67	K	100.0 .. 350.0	12	32	265
Cloud effective altitude: mean, std, num obs	68	km	0.0 .. 20.0	12	32	277
Cloud top pressure: mean, std, num obs	69	hPa	0.0 .. 1100.0	12	32	289
Cloud bottom pressure: mean, std, num obs	70	hPa	0.0 .. 1100.0	12	32	301
Cloud particle phase: mean, std, num obs	71	Fraction	0.0 .. 1.0	12	32	313
Liquid water path: mean, std, num obs	72	kg m^{-2}	0.01 .. 1000.0	12	32	325
Ice water path: mean, std, num obs	73	kg m^{-2}	0.01 .. 1000.0	12	32	337
Liquid particle radius: mean, std, num obs	74	micron	0.0 .. 1000.0	12	32	349
Ice particle effective diameter: mean, std, num obs	75	micron	0.0 .. 100.0	12	32	361
Visible optical depth (linear): mean, std, num obs	76	Dimensionless	0.0 .. 50.0	12	32	373
Visible optical depth (logarithmic): mean, std, num obs	77	Dimensionless	0.0 .. 50.0	12	32	385
Infrared emissivity: mean, std, num obs	78	Dimensionless	0.0 .. 2.0	12	32	397
Cloud vertical aspect ratio: mean, std, num obs	79	Dimensionless	TBD	12	32	409
Spatially Averaged Adjustment Parameters						
Adjusted visible optical depth: mean, std	80	Dimensionless	0.0 .. 400.0	8	32	421
Adjusted cloud fractional area: mean, std	81	Dimensionless	0.0 .. 100.0	8	32	429
Adjusted infrared emissivity: mean, std	82	Dimensionless	0.0 .. 1.0	8	32	437
Adjusted cloud effective temperature: mean, std	83	K	0.0 .. 250.0	8	32	445
Spatially Averaged Weighted Column						
Averaged Cloud Properties for 5 Weightings						
(Five Weightings: SW, LW TOA, SFC LW, LWP, IWP)						
Spatially Averaged Cloud Area Fractions						
Overcast percent coverage	84	Percent	0.0 .. 100.0	5	32	453
Total percent coverage	85	Percent	0.0 .. 100.0	5	32	458
Spatially Averaged Cloud Properties is Array[3] of:						
Cloud effective pressure: mean, std, num obs	86	hPa	0.0 .. 1100.0	15	32	463
Cloud effective temperature: mean, std, num obs	87	K	100.0 .. 350.0	15	32	478

Description	Parameter Num	Unit	Range	Elements/ Record	Bits/ Elem	Elem Num
Cloud effective altitude: mean, std, num obs	88	km	0.0 .. 20.0	15	32	493
Cloud top pressure: mean, std, num obs	89	hPa	0.0 .. 1100.0	15	32	508
Cloud bottom pressure: mean, std, num obs	90	hPa	0.0 .. 1100.0	15	32	523
Cloud particle phase: mean, std, num obs	91	Fraction	0.0 .. 1.0	15	32	538
Liquid water path: mean, std, num obs	92	kg m^{-2}	0.01 .. 1000.0	15	32	553
Ice water path: mean, std, num obs	93	kg m^{-2}	0.01 .. 1000.0	15	32	568
Liquid particle radius: mean, std, num obs	94	micron	0.0 .. 1000.0	15	32	583
Ice particle effective diameter: mean, std, num obs	95	micron	0.0 .. 100.0	15	32	598
Visible optical depth (linear): mean, std, num obs	96	Dimensionless	0.0 .. 50.0	15	32	613
Visible optical depth (logarithmic): mean, std, num obs	97	Dimensionless	0.0 .. 50.0	15	32	628
Infrared emissivity: mean, std, num obs	98	Dimensionless	0.0 .. 2.0	15	32	643
Cloud vertical aspect ratio: mean, std, num obs	99	Dimensionless	TBD	15	32	658
Spatially Averaged Angular Model Scene Type Parameters						
Angular Model Scene Type Parameters for 12 Scene Types						
Fractional area coverage	100	Percent	0.0 .. 100.0	12	32	673
Angular Model Scene Type Statistical Data is Array[2] of:						
Incident Solar Flux: mean, std	101	Dimensionless	0.0 .. 1400.0	24	32	685
Albedo: mean, std	102	Dimensionless	0.0 .. 1.0	24	32	709
LW flux: mean, std	103	W m^{-2}	0.0 .. 400.0	24	32	733
Spatially Averaged Clear Sky Adjustment Parameters						
Adjusted precipitable water: mean, std	104	cm	0.001 .. 8.0	2	32	757
Adjusted surface albedo: mean, std	105	Dimensionless	0.0 .. 1.0	2	32	759
Adjusted aerosol optical depth: mean, std	106	Dimensionless	0.0 .. 2.0	2	32	761
Adjusted skin temperature: mean, std	107	K	TBD	2	32	763
Spatially Average Surface Data						
Spectral Reflectivity: mean, std, num obs	108	Dimensionless	0.0 .. 1.0	3	32	765
Broadband Surface Albedo: mean, std, num obs	109	Dimensionless	0.0 .. 1.0	3	32	768
Surface Skin Temperature: mean, std, num obs	110	K	175.0 .. 375.0	3	32	771

Total Meta Bits/File:	11848
Total Data Bits/Record:	24736
Total Records/File:	23572
Total Data Bits/File:	583076992
Total Bits/File:	583088840

Total Files/Product:	180
Total Meta Bits/Product:	2132640
Total Data Bits/Product:	104953858560
Total Bits/Product:	104955991200

Total MegaBytes/File:	69.51
Total GigaBytes/Product:	12.22

Appendix B

Output Data Products

Merge Satellites, Time Interpolate, Compute Fluxes (Subsystem 7.0)

This appendix describes the data products which are produced by the algorithms in this subsystem. Table B-1 below summarizes these products, listing the CERES and EOSDIS product codes or abbreviations, a short product name, the product category, the production frequency, and volume estimates for each individual product as well as a complete data month of production. The product categories are defined as follows:

Archival products: Assumed to be permanently stored by EOSDIS
Internal products: Temporary storage by EOSDIS (days to years)

The following pages describe each product. An introductory page provides an overall description of the product and specifies the temporal and spatial coverage. The table which follows the introductory page briefly describes every parameter which is contained in the product. Each product may be thought of as metadata followed by data records. The metadata (or header data) is not well-defined yet and is included mainly as a placeholder. The description of parameters which are present in each data record includes parameter number (a unique number for each distinct parameter), units, dynamic range, the number of elements per record, an estimate of the number of bits required to represent each parameter, and an element number (a unique number for each instance of every parameter). A summary at the bottom of each table shows the current estimated size of metadata, each data record, and the total data product. A more detailed description of each data product will be contained in a user's guide to be published before the first CERES launch.

Table B-1. Output Products Summary

Product code		Name	Type	Frequency	Size, MB	Monthly size, MB
CERES	EOSDIS					
SYN	CER07	Synoptic Radiative Fluxes and Clouds	Archival	Every 3 Hours	145.23	36016

Synoptic Radiative Fluxes and Clouds (SYN)

The Synoptic Radiative Fluxes and Clouds (SYN), a CERES archival product, is produced by the CERES Merge Satellites, Time Interpolate, Compute Fluxes Subsystem. Each SYN file contains regional longwave and shortwave radiative fluxes for the surface, internal atmosphere and TOA. The data are computed at 3-hour intervals on the CERES grid, and are based on measurements from multiple EOS CERES instruments. In addition to being an archival product, the SYN is used by the CERES subsystem, Compute Regional, Zonal and Global Averages.

The SYN contains averaged:

- Regional data
- Clear-sky area scene data
- Observed CERES TOA data
- Cloud category properties for four (low, lower middle, upper middle and high) cloud height categories
- Column averaged cloud properties for five (TOA SW, TOA LW, SFC LW, LWC and IWC) weighting schemes

- Overlap data for eleven (clear, low (L), lower middle (LM), upper middle (UM), high (H), H/UM, H/LM, H/L, UM/LM, UM/L, LM/L) cloud overlap conditions
- Angular model scene classes for the twelve ERBE scene types
- Surface radiative parameters
- Untuned radiative fluxes for both clear skies and total scene at the surface and the TOA
- Tuned radiative fluxes for both clear skies and total scene at the surface, 500hPa, the tropopause and the TOA
- Adjustment parameters for clear skies
- Adjustment parameters for four (low, lower middle, upper middle and high) cloud height categories

Level: 3
Type: Archival
Frequency: Every 3 Hours

Time Interval Covered
File: 3 Hours
Record: 3 Hours

Portion of Globe Covered
File: Global
Record: 1 CERES region

Portion of Atmosphere Covered
File: Surface, Internal and TOA

Table B-2. Synoptic Radiative Fluxes and Clouds (SYN) Page 1 of 3

Description	Parameter Number	Units	Range	Elements/ Record	Bits/ Elem	Elem Num
Meta Data						
SYN Header FIle		N/A		1	380	
Regional Data						
Julian date at hour start	1	day	2449395 .. 2456000	1	32	1
Julian time at hour start	2	day	0 .. 1	1	32	2
Region number	3	N/A	1 .. 64800	1	32	3
Hour-box number	4	N/A	1 .. 744	1	32	4
Surface altitude above sea level, mean	5	m	-1000 .. 10000	1	32	5
Precipitable water	6	cm	0.001 .. 10.000	1	32	6
Cosine of solar zenith angle	7	deg	0 .. 1	1	32	7
Surface type percent coverage	8	N/A	0 .. 100	20	32	8
Clear-sky Area Data						
Snow/ice percent coverage	9	N/A	0 .. 100	1	32	28
Smoke percent coverage	10	N/A	0 .. 100	1	32	29
Fire percent coverage	11	N/A	0 .. 100	1	32	30
Total aerosol visible optical depth, clear area	12	N/A	0 .. 2	1	32	31
Total aerosol effective radius, clear area	13	N/A	0 .. 20	1	32	32
Observed CERES TOA Data for Clear-sky and Total-sky						
CERES SW flux, TOA, upwards, mean	14	$W\ m^{-2}$	0 .. 1400	2	32	33
CERES SW flux, TOA, upwards, std	15	$W\ m^{-2}$	TBD	2	32	35
CERES LW flux, TOA, upwards, mean	16	$W\ m^{-2}$	0 .. 1000	2	32	37
CERES LW flux, TOA, upwards, std	17	$W\ m^{-2}$	TBD	2	32	39
CERES WN flux, TOA, upwards, mean	18	$W\ m^{-2}$	10 .. 400	2	32	41
CERES WN flux, TOA, upwards, std	19	$W\ m^{-2}$	TBD	2	32	43
Albedo, TOA, mean	20	N/A	0 .. 1	2	32	45
Albedo, TOA, std	21	N/A	0 .. 1	2	32	47
Cloud Properties for 4 Cloud Height Categories (Cloud height categories are low, lower middle, upper middle and high)						
Overcast cloud area percentage	22	N/A	0 .. 100	4	32	49
Total cloud area percentage	23	N/A	0 .. 100	4	32	53
Cloud visible optical depth, mean	24	N/A	0 .. 400	4	32	57
Cloud vsible optical depth, std	25	N/A	TBD	4	32	61
Cloud infrared emissivity, mean	26	N/A	0 .. 1	4	32	65
Cloud infrared emissivity, std	27	N/A	0 .. 1	4	32	69
Cloud liquid water path, mean	28	$g\ m^{-2}$	0.001 .. 10.00	4	32	73
Cloud liquid water path, std	29	$g\ m^{-2}$	TBD	4	32	77
Cloud ice water path, mean	30	$g\ m^{-2}$	0.001 .. 10.00	4	32	81
Cloud ice water path, std	31	$g\ m^{-2}$	TBD	4	32	85
Cloud top pressure, mean	32	hPa	0 .. 1100	4	32	89
Cloud top pressure, std	33	hPa	TBD	4	32	93
Cloud effective pressure, mean	34	hPa	0 .. 1100	4	32	97
Cloud effective pressure, std	35	hPa	TBD	4	32	101
Cloud effective temperature, mean	36	K	100 .. 350	4	32	105
Cloud effective temperature, std	37	K	TBD	4	32	109
Cloud effective height, mean	38	km	0 .. 20	4	32	113
Cloud effective height, std	39	km	TBD	4	32	117
Cloud bottom pressure, mean	40	hPa	0 .. 1100	4	32	121
Cloud bottom pressure, std	41	hPa	TBD	4	32	125
Cloud liquid particle radius, mean	42	µm	0 .. 200	4	32	129
Cloud liquid particle radius, std	43	µm	TBD	4	32	133
Cloud ice particle effective diameter, mean	44	µm	0 .. 200	4	32	137
Cloud ice particle effective diameter, std	45	µm	TBD	4	32	141
Cloud particle phase, mean	46	N/A	0 .. 1	4	32	145
Cloud particle phase, std	47	N/A	0 .. 1	4	32	149
Vertical aspect ratio, mean	48	N/A	0 .. 1	4	32	153
Vertical aspect ratio, std	49	N/A	0 .. 1	4	32	157
Visible optical depth, 13 percentiles	50	N/A	TBD	52	32	161
Infrared emissivity, 13 percentiles	51	N/A	TBD	52	32	213

Table B-2. Synoptic Radiative Fluxes and Clouds (SYN) Page 2 of 3

Description	Parameter Number	Units	Range	Elements/ Record	Bits/ Elem	Elem Num
Column Averaged Cloud Properties for TOA-SW, TOA-LW, SFC-LW, LWC and IWC Weighting Schemes						
Overcast cloud area percentage	52	N/A	0 .. 100	5	32	265
Total cloud area percentage	53	N/A	0 .. 100	5	32	270
Cloud visible optical depth, mean	54	N/A	0 .. 400	5	32	275
Cloud vsible optical depth, std	55	N/A	TBD	5	32	280
Cloud infrared emissivity, mean	56	N/A	0 .. 1	5	32	285
Cloud infrared emissivity, std	57	N/A	0 .. 1	5	32	290
Cloud liquid water path, mean	58	g m^{-2}	0.001 .. 10.00	5	32	295
Cloud liquid water path, std	59	g m^{-2}	TBD	5	32	300
Cloud ice water path, mean	60	g m^{-2}	0.001 .. 10.00	5	32	305
Cloud ice water path, std	61	g m^{-2}	TBD	5	32	310
Cloud top pressure, mean	62	hPa	0 .. 1100	5	32	315
Cloud top pressure, std	63	hPa	TBD	5	32	320
Cloud effective pressure, mean	64	hPa	0 .. 1100	5	32	325
Cloud effective pressure, std	65	hPa	TBD	5	32	330
Cloud effective temperature, mean	66	K	100 .. 350	5	32	335
Cloud effective temperature, std	67	K	TBD	5	32	340
Cloud effective height, mean	68	km	0 .. 20	5	32	345
Cloud effective height, std	69	km	TBD	5	32	350
Cloud bottom pressure, mean	70	hPa	0 .. 1100	5	32	355
Cloud bottom pressure, std	71	hPa	TBD	5	32	360
Cloud liquid particle radius, mean	72	µm	0 .. 200	5	32	365
Cloud liquid particle radius, std	73	µm	TBD	5	32	370
Cloud ice particle effective diameter, mean	74	µm	0 .. 200	5	32	375
Cloud ice particle effective diameter, std	75	µm	TBD	5	32	380
Cloud particle phase, mean	76	N/A	0 .. 1	5	32	385
Cloud vertical aspect ratio, mean	77	N/A	0 .. 1	5	32	390
Cloud vertical aspect ratio, std	78	N/A	0 .. 1	5	32	395
Overlap Footprint Data for 11 Cloud Overlap Conditions (Cloud classes are clear, low (L), lower middle (LM), upper middle (UM), high (H), H/UM, H/LM, H/L, UM/LM, UM/L, and LM/L)						
Overlap condition weighted area percentage	79	N/A	0 .. 100	11	32	400
Angular Model Scene Classes for 12 ERBE Scene Types						
Fractional area coverage	80	N/A	0 .. 1	12	32	411
Albedo, mean	81	N/A	0 .. 1	12	32	423
Albedo, std	82	N/A	0 .. 1	12	32	435
Incident solar flux	83	W m^{-2}	TBD	12	32	447
Longwave flux, mean	84	W m^{-2}	TBD	12	32	459
Longwave flux, std	85	W m^{-2}	TBD	12	32	471
Surface Radiative Parameters						
Spectral reflectivity	86	N/A	0 .. 1	6	32	483
Broadband surface albedo	87	N/A	0 .. 1	1	32	489
LW surface emissivity	88	N/A	0 .. 1	1	32	490
WN surface emissivity	89	N/A	0 .. 1	1	32	491
Imager-based surface skin temperature	90	K	175 .. 375	1	32	492
Photosynthetically active radiation	91	W m^{-2}	0 .. 780	1	32	493
DIrect/diffuse ratio	92	N/A	0 .. 30	1	32	494
Atmospheric Flux Profile for Clear-sky and Total-sky (Atmospheric levels in profile are surface, 500hPa, tropopause and TOA)						
Number atmospheric levels	93	N/A	0 .. 4	1	32	495
Pressure, atmospheric levels	94	hPa	0 .. 1100	4	32	496
SW flux, atmospheric level, upwards, tuned	95	W m^{-2}	0 .. 1400	8	32	500
SW flux, atmospheric level, downwards, tuned	96	W m^{-2}	0 .. 1400	8	32	508
LW flux, atmospheric level, upwards, tuned	97	W m^{-2}	0 .. 1000	8	32	516
LW flux, atmospheric level, downwards, tuned	98	W m^{-2}	0 .. 1000	8	32	524

Table B-2. Synoptic Radiative Fluxes and Clouds (SYN) Page 3 of 3

Description	Parameter Number	Units	Range	Elements/ Record	Bits/ Elem	Elem Num
Flux Adjustments (Tuned - Untuned) for Clear-sky and Total-sky at Surface and TOA						
Number of tuning iterations	99	N/A	0 .. 3	1	16	532
SW flux, surface, downwards, delta	100	W m^{-2}	0 .. 1400	2	32	533
SW flux, surface, upwards, delta	101	W m^{-2}	0 .. 1400	2	32	535
SW flux, TOA, upwards, delta	102	W m^{-2}	0 .. 1400	2	32	537
SW flux, TOA, downwards, delta	103	W m^{-2}	0 .. 1400	2	32	539
LW flux, surface, downwards, delta	104	W m^{-2}	0 .. 1000	2	32	541
LW flux, surface, upwards, delta	105	W m^{-2}	0 .. 1000	2	32	543
LW flux, TOA, upwards, delta	106	W m^{-2}	0 .. 1000	2	32	545
Adjustment Parameters for Clear Skies						
Adjusted precipitable water, delta	107	cm	0.001 .. 10.000	1	32	495
Adjusted surface albedo, delta	108	N/A	0 .. 1	1	32	496
Adjusted aerosol optical depth, delta	109	N/A	0.0 .. 2.0	1	32	497
Adjusted skin temperature, delta	110	K	TBD	1	32	498
Adjustment Parameters for 4 Cloud Height Categories						
Adjusted mean visible optical depth, delta	111	N/A	0 .. 400	4	32	499
Adjusted std visible optical depth	112	N/A	TBD	4	32	503
Adjusted mean cloud fractional area, delta	113	N/A	0 .. 1	4	32	507
Adjusted std cloud fractional area	114	N/A	0 .. 1	4	32	511
Adjusted mean cloud infrared emissivity, delta	115	N/A	0 .. 1	4	32	515
Adjusted std cloud infrared emissivity	116	N/A	0 .. 1	4	32	519
Adjusted mean cloud effective temperature, delta	117	K	0 .. 250	4	32	523
Adjusted std cloud effective temperature	118	K	TBD	4	32	527

Total Meta Bits/File:	380
Total Data Bits/Record:	18800
Total Records/File:	64800
Total Data Bits/File:	1218240000
Total Bits/File:	1218240380

Appendix C

Nomenclature

Acronyms

ADEOS	Advanced Earth Observing System
ADM	Angular Distribution Model
AIRS	Atmospheric Infrared Sounder (EOS-AM)
AMSU	Advanced Microwave Sounding Unit (EOS-PM)
APD	Aerosol Profile Data
APID	Application Identifier
ARESE	ARM Enhanced Shortwave Experiment
ARM	Atmospheric Radiation Measurement
ASOS	Automated Surface Observing Sites
ASTER	Advanced Spaceborne Thermal Emission and Reflection Radiometer
ASTEX	Atlantic Stratocumulus Transition Experiment
ASTR	Atmospheric Structures
ATBD	Algorithm Theoretical Basis Document
AVG	Monthly Regional, Average Radiative Fluxes and Clouds (CERES Archival Data Product)
AVHRR	Advanced Very High Resolution Radiometer
BDS	Bidirectional Scan (CERES Archival Data Product)
BRIE	Best Regional Integral Estimate
BSRN	Baseline Surface Radiation Network
BTD	Brightness Temperature Difference(s)
CCD	Charge Coupled Device
CCSDS	Consultative Committee for Space Data Systems
CEPEX	Central Equatorial Pacific Experiment
CERES	Clouds and the Earth’s Radiant Energy System
CID	Cloud Imager Data
CLAVR	Clouds from AVHRR
CLS	Constrained Least Squares
COPRS	Cloud Optical Property Retrieval System
CPR	Cloud Profiling Radar
CRH	Clear Reflectance, Temperature History (CERES Archival Data Product)
CRS	Single Satellite CERES Footprint, Radiative Fluxes and Clouds (CERES Archival Data Product)
DAAC	Distributed Active Archive Center
DAC	Digital-Analog Converter
DAO	Data Assimilation Office

DB	Database
DFD	Data Flow Diagram
DLF	Downward Longwave Flux
DMSP	Defense Meteorological Satellite Program
EADM	ERBE-Like Albedo Directional Model (CERES Input Data Product)
ECA	Earth Central Angle
ECLIPS	Experimental Cloud Lidar Pilot Study
ECMWF	European Centre for Medium-Range Weather Forecasts
EDDB	ERBE-Like Daily Data Base (CERES Archival Data Product)
EID9	ERBE-Like Internal Data Product 9 (CERES Internal Data Product)
EOS	Earth Observing System
EOSDIS	Earth Observing System Data Information System
EOS-AM	EOS Morning Crossing Mission
EOS-PM	EOS Afternoon Crossing Mission
ENSO	El Niño/Southern Oscillation
ENVISAT	Environmental Satellite
EPHANC	Ephemeris and Ancillary (CERES Input Data Product)
ERB	Earth Radiation Budget
ERBE	Earth Radiation Budget Experiment
ERBS	Earth Radiation Budget Satellite
ESA	European Space Agency
ES4	ERBE-Like S4 Data Product (CERES Archival Data Product)
ES4G	ERBE-Like S4G Data Product (CERES Archival Data Product)
ES8	ERBE-Like S8 Data Product (CERES Archival Data Product)
ES9	ERBE-Like S9 Data Product (CERES Archival Data Product)
FLOP	Floating Point Operation
FIRE	First ISCCP Regional Experiment
FIRE II IFO	First ISCCP Regional Experiment II Intensive Field Observations
FOV	Field of View
FSW	Hourly Gridded Single Satellite Fluxes and Clouds (CERES Archival Data Product)
FTM	Functional Test Model
GAC	Global Area Coverage (AVHRR data mode)
GAP	Gridded Atmospheric Product (CERES Input Data Product)
GCIP	GEWEX Continental-Phase International Project
GCM	General Circulation Model
GEBA	Global Energy Balance Archive
GEO	ISSCP Radiances (CERES Input Data Product)
GEWEX	Global Energy and Water Cycle Experiment
GLAS	Geoscience Laser Altimetry System

GMS	Geostationary Meteorological Satellite
GOES	Geostationary Operational Environmental Satellite
HBTM	Hybrid Bispectral Threshold Method
HIRS	High-Resolution Infrared Radiation Sounder
HIS	High-Resolution Interferometer Sounder
ICM	Internal Calibration Module
ICRCCM	Intercomparison of Radiation Codes in Climate Models
ID	Identification
IEEE	Institute of Electrical and Electronics Engineers
IES	Instrument Earth Scans (CERES Internal Data Product)
IFO	Intensive Field Observation
INSAT	Indian Satellite
IOP	Intensive Observing Period
IR	Infrared
IRIS	Infrared Interferometer Spectrometer
ISCCP	International Satellite Cloud Climatology Project
ISS	Integrated Sounding System
IWP	Ice Water Path
LAC	Local Area Coverage (AVHRR data mode)
LaRC	Langley Research Center
LBC	Laser Beam Ceilometer
LBTM	Layer Bispectral Threshold Method
Lidar	Light Detection and Ranging
LITE	Lidar In-Space Technology Experiment
Lowtran 7	Low-Resolution Transmittance (Radiative Transfer Code)
LW	Longwave
LWP	Liquid Water Path
MAM	Mirror Attenuator Mosaic
MC	Mostly Cloudy
MCR	Microwave Cloud Radiometer
METEOSAT	Meteorological Operational Satellite (European)
METSAT	Meteorological Satellite
MFLOP	Million FLOP
MIMR	Multifrequency Imaging Microwave Radiometer
MISR	Multiangle Imaging Spectroradiometer
MLE	Maximum Likelihood Estimate
MOA	Meteorology Ozone and Aerosol
MODIS	Moderate-Resolution Imaging Spectroradiometer
MSMR	Multispectral, Multiresolution

MTSA	Monthly Time and Space Averaging
MWH	Microwave Humidity
MWP	Microwave Water Path
NASA	National Aeronautics and Space Administration
NCAR	National Center for Atmospheric Research
NCEP	National Centers for Environmental Prediction
NESDIS	National Environmental Satellite, Data, and Information Service
NIR	Near Infrared
NMC	National Meteorological Center
NOAA	National Oceanic and Atmospheric Administration
NWP	Numerical Weather Prediction
OLR	Outgoing Longwave Radiation
OPD	Ozone Profile Data (CERES Input Data Product)
OV	Overcast
PC	Partly Cloudy
POLDER	Polarization of Directionality of Earth's Reflectances
PRT	Platinum Resistance Thermometer
PSF	Point Spread Function
PW	Precipitable Water
RAPS	Rotating Azimuth Plane Scan
RPM	Radiance Pairs Method
RTM	Radiometer Test Model
SAB	Sorting by Angular Bins
SAGE	Stratospheric Aerosol and Gas Experiment
SARB	Surface and Atmospheric Radiation Budget Working Group
SDCD	Solar Distance Correction and Declination
SFC	Hourly Gridded Single Satellite TOA and Surface Fluxes (CERES Archival Data Product)
SHEBA	Surface Heat Budget in the Arctic
SPECTRE	Spectral Radiance Experiment
SRB	Surface Radiation Budget
SRBAVG	Surface Radiation Budget Average (CERES Archival Data Product)
SSF	Single Satellite CERES Footprint TOA and Surface Fluxes, Clouds
SSMI	Special Sensor Microwave Imager
SST	Sea Surface Temperature
SURFMAP	Surface Properties and Maps (CERES Input Product)
SW	Shortwave
SWICS	Shortwave Internal Calibration Source
SYN	Synoptic Radiative Fluxes and Clouds (CERES Archival Data Product)

SZA	Solar Zenith Angle
THIR	Temperature/Humidity Infrared Radiometer (Nimbus)
TIROS	Television Infrared Observation Satellite
TISA	Time Interpolation and Spatial Averaging Working Group
TMI	TRMM Microwave Imager
TOA	Top of the Atmosphere
TOGA	Tropical Ocean Global Atmosphere
TOMS	Total Ozone Mapping Spectrometer
TOVS	TIROS Operational Vertical Sounder
TRMM	Tropical Rainfall Measuring Mission
TSA	Time-Space Averaging
UAV	Unmanned Aerospace Vehicle
UT	Universal Time
UTC	Universal Time Code
VAS	VISSR Atmospheric Sounder (GOES)
VIRS	Visible Infrared Scanner
VISSR	Visible and Infrared Spin Scan Radiometer
WCRP	World Climate Research Program
WG	Working Group
Win	Window
WN	Window
WMO	World Meteorological Organization
ZAVG	Monthly Zonal and Global Average Radiative Fluxes and Clouds (CERES Archival Data Product)

Symbols

A	atmospheric absorptance
$B_\lambda(T)$	Planck function
C	cloud fractional area coverage
CF_2Cl_2	dichlorofluorocarbon
$CFCl_3$	trichlorofluorocarbon
CH_4	methane
CO_2	carbon dioxide
D	total number of days in the month
D_e	cloud particle equivalent diameter (for ice clouds)
E_o	solar constant or solar irradiance
F	flux
f	fraction
G_a	atmospheric greenhouse effect

g	cloud asymmetry parameter
H_2O	water vapor
I	radiance
i	scene type
m_i	imaginary refractive index
$\hat{N}$	angular momentum vector
N_2O	nitrous oxide
O_3	ozone
P	point spread function
p	pressure
Q_a	absorption efficiency
Q_e	extinction efficiency
Q_s	scattering efficiency
R	anisotropic reflectance factor
r_E	radius of the Earth
r_e	effective cloud droplet radius (for water clouds)
r_h	column-averaged relative humidity
S_o	summed solar incident SW flux
S_o'	integrated solar incident SW flux
T	temperature
T_B	blackbody temperature
t	time or transmittance
W_{liq}	liquid water path
w	precipitable water
$\hat{x}_o$	satellite position at t_o
x, y, z	satellite position vector components
$\dot{x}, \dot{y}, \dot{z}$	satellite velocity vector components
z	altitude
z_{top}	altitude at top of atmosphere
α	albedo or cone angle
β	cross-scan angle
γ	Earth central angle
γ_{at}	along-track angle
γ_{ct}	cross-track angle
δ	along-scan angle
ε	emittance
Θ	colatitude of satellite
θ	viewing zenith angle
θ_o	solar zenith angle

λ	wavelength
μ	viewing zenith angle cosine
μ_o	solar zenith angle cosine
ν	wave number
ρ	bidirectional reflectance
τ	optical depth
$\tau_{aer}(p)$	spectral optical depth profiles of aerosols
$\tau_{H_2O\lambda}(p)$	spectral optical depth profiles of water vapor
$\tau_{O_3}(p)$	spectral optical depth profiles of ozone
Φ	longitude of satellite
ϕ	azimuth angle
$\tilde{\omega}_o$	single-scattering albedo

Subscripts:

c	cloud
cb	cloud base
ce	cloud effective
cld	cloud
cs	clear sky
ct	cloud top
ice	ice water
lc	lower cloud
liq	liquid water
s	surface
uc	upper cloud
λ	spectral wavelength

Units

AU	astronomical unit
cm	centimeter
cm-sec^{-1}	centimeter per second
count	count
day	day, Julian date
deg	degree
deg-sec^{-1}	degree per second
DU	Dobson unit
erg-sec^{-1}	erg per second
fraction	fraction (range of 0–1)
g	gram
g-cm^{-2}	gram per square centimeter

$g\text{-}g^{-1}$	gram per gram
$g\text{-}m^{-2}$	gram per square meter
h	hour
hPa	hectopascal
K	Kelvin
kg	kilogram
$kg\text{-}m^{-2}$	kilogram per square meter
km	kilometer
$km\text{-}sec^{-1}$	kilometer per second
m	meter
mm	millimeter
μm	micrometer, micron
N/A	not applicable, none, unitless, dimensionless
$ohm\text{-}cm^{-1}$	ohm per centimeter
percent	percent (range of 0–100)
rad	radian
$rad\text{-}sec^{-1}$	radian per second
sec	second
sr^{-1}	per steradian
W	watt
$W\text{-}m^{-2}$	watt per square meter
$W\text{-}m^{-2}sr^{-1}$	watt per square meter per steradian
$W\text{-}m^{-2}sr^{-1}\mu m^{-1}$	watt per square meter per steradian per micrometer